NASA TECHNICAL MEMORANDUM

NASA TM X-62,124

NASA TM X-62,124

BALLISTIC RANGE MEASUREMENTS OF THE DRAG AND STATIC AND DYNAMIC STABILITY OF A RECOVERABLE SPACE SHUTTLE BOOSTER VEHICLE

Peter F. Intrieri and Donn B. Kirk

Ames Research Center
Moffett Field, Calif. 94035

May 1972

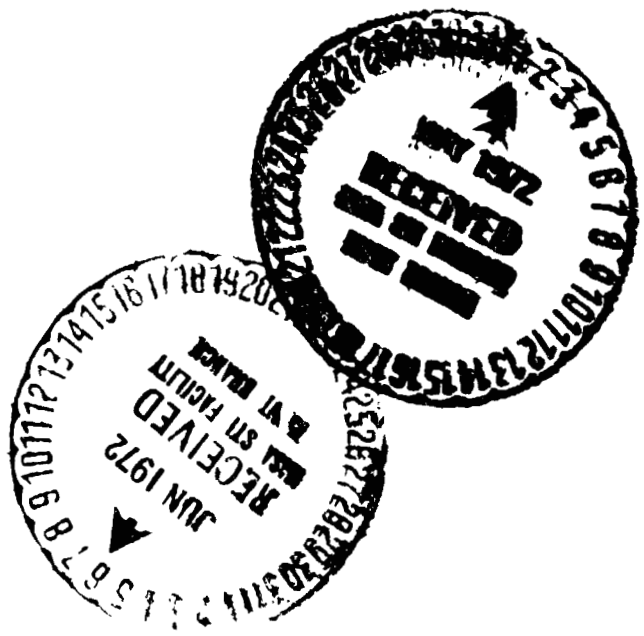

BALLISTIC RANGE MEASUREMENTS OF THE DRAG AND STATIC AND DYNAMIC STABILITY OF A RECOVERABLE SPACE SHUTTLE BOOSTER VEHICLE

Peter F. Intrieri and Donn B. Kirk

Ames Research Center

ABSTRACT

An experimental study has been conducted in the Ames Pressurized Ballistic Range to determine the aerodynamic characteristics of a proposed recoverable space shuttle booster vehicle. Tests were made at Mach numbers of 0.7, 1.5, and 3.5 of two configurations, one with tail panels deflected 90° and one with tail panels deflected 70°. Both configurations were found to be highly statically stable at all Mach numbers. The dynamic behavior was erratic; the models exhibited both neutral dynamic stability and dynamic instability, and the motions experienced during free flight at the subsonic Mach number were very irregular. The flow field over the models was characterized by an extensive separated-flow region which largely encompassed the tail panels. The experimental drag and static stability were not well predicted by available theoretical estimates.

BALLISTIC RANGE MEASUREMENTS OF THE DRAG AND STATIC AND DYNAMIC STABILITY OF A RECOVERABLE SPACE SHUTTLE BOOSTER VEHICLE

Peter F. Intrieri and Donn B. Kirk

Ames Research Center

SUMMARY

An exploratory experimental study has been conducted in a ballistic range to determine the levels of drag and static and dynamic stability of a proposed recoverable space shuttle booster vehicle at Mach numbers of 0.7, 1.5, and 3.5. Two configurations were tested, one with tail panels deflected 90° and one with tail panels deflected 70°. This change in sweepback angle of the tail panels had little effect on the drag or static and dynamic stability of the vehicle at all Mach numbers of this investigation. Both configurations were statically stable at all Mach numbers investigated. The dynamic behavior of these configurations was erratic; four of the flights indicated essentially neutral dynamic stability, and the remaining four flights indicated dynamic instability. The flow field over the models is characterized by an extensive separated-flow region which largely encompasses the tail panels of both configurations. This separated flow undoubtedly influences the drag and static- and dynamic-stability characteristics of the configurations and causes the motions of the models during free flight to be very irregular, particularly at the subsonic Mach number. The drag and static stability of these configurations were not well predicted by available

empirical and theoretical estimates. The results of one flight of a 70°-panel model, launched backwards at a Mach number of 2.5, indicated this configuration is not statically stable about this backward orientation at the present test conditions.

INTRODUCTION

NASA is currently engaged in a major effort to provide the technology necessary for the design, fabrication, and operation of a space shuttle system (orbiter and booster) capable of transporting personnel and supplies to low Earth orbit, with the orbiter returning using conventional airplane-type landings. The unmanned booster could be recovered by means of an aerodynamically passive reentry system. A possible candidate for use as a passive, recoverable space shuttle booster vehicle is shown in figure 1. This configuration is applicable to both a pressure-fed or solid rocket motor booster system and consists of a blunt cone forebody, a long cylindrical body, and eight relatively large tail panels. In the launch configuration the tail panels would be folded into, and actually form, the aft portion of the booster. At the prescribed altitude the orbiter would separate from the booster and continue to a low Earth orbit. The booster with fuel expended would deploy its tail panels, reorient itself nose forward, and descend through the atmosphere with the tail panels providing high drag to decelerate the vehicle to an acceptably low speed upon impact into the sea, where final recovery would be accomplished by a ship.

Having established, in concept, the feasibility of such a passive booster system, it must be ascertained that the drag of the configuration will be sufficiently high to decelerate the vehicle to an acceptable terminal speed, and that the stability will be adequate to insure proper orientation of the vehicle during the entry. In addition, it is particularly important that the vehicle's dynamic stability will be sufficient to prevent divergent oscillations which could lead to unsuccessful recovery.

The present exploratory investigation was undertaken to determine the drag and static- and dynamic-stability characteristics of the two configurations shown in figure 2. The purpose of this report is to present the results of this investigation. The tests were conducted in air in the Ames Pressurized Ballistic Range at nominal Mach numbers of 0.7, 1.5, and 3.5, with corresponding Reynolds numbers of 0.3, 0.6, and 1.5 million based on free-stream conditions and model cylinder diameter. Two configurations were tested, one with the tail panels deflected 90° and one with the tail panels deflected 70°. One flight was also made with the 70°-panel model launched backwards to determine whether it would remain flying backward or would begin righting itself to a nose-forward attitude. Wherever possible, the present experimental results are compared with available empirical and theoretical estimates.

SYMBOLS

A	reference area (cylinder cross-sectional area)
C_D	drag coefficient
C_{L_α}	lift-curve slope
C_{m_α}	quasi-linear pitching-moment-curve slope
$C_{m_q} + C_{m_{\dot{\alpha}}}$	damping-in-pitch derivative
d	reference length (model cylinder diameter)
I_Y	moment of inertia about a transverse axis through the center of gravity
ℓ	model length
M	Mach number
m	model mass
p	roll rate about axis of symmetry of model
t	time
V	free-stream velocity
x	distance flown
x_{cg}	axial distance from model nose to center of gravity
y	horizontal coordinate normal to the flightpath
z	coordinate normal to the flightpath and y-axis
α	angle of attack (in the vertical plane)
β	angle of sideslip (in the horizontal plane)
η_1, η_2	damping exponents in equation (3)
θ	angular displacement measured in the xz plane

λ	wavelength of pitching oscillation
ξ	dynamic-stability parameter for unpowered flight at constant altitude
ρ	free-stream air density
σ	resultant angle of attack
ψ	angular displacement measured in the xy plane
ω_1, ω_2	rates of rotation of vectors that describe the model oscillatory motion in equation (3)

DESCRIPTION OF TESTS

Test Technique and Test Conditions

The tests were performed in the Ames Pressurized Ballistic Range by launching models from a 57-mm smooth-bore powder-gas gun into still air at ambient temperature. Nominal model velocities of 250, 500, and 1200 m/sec were obtained corresponding to nominal Mach numbers of 0.7, 1.5, and 3.5, respectively. The test section static pressure was one atmosphere, which gave Reynolds numbers of 0.3, 0.6, and 1.5 million, respectively, based on model cylinder diameter. (Note that the full-scale Reynolds numbers would be in the range of 50 to 75 million at these Mach numbers.)

The trajectory of the models through the test section was recorded over a 62-m (203-foot) flightpath in 24 shadowgraph stations located at various intervals. Side and plan views of the model are recorded in each shadowgraph, along with reference wires from which x, y, z, θ and ψ coordinates could be read; the linear coordinates are accurate to 0.01 cm, and angles to within 0.25°. The orientation angles, θ and ψ, were read

relative to Earth-fixed axes. Corrections to θ and ψ were made to account for the angles between the resultant instantaneous velocity vector and the Earth-fixed axes and thus to give values of α and β. Times of model flight between stations were recorded with electronic chronographs to within 5/8 μsec.

Models and Sabots

Sketches of the models showing pertinent nominal dimensions are shown in figure 2. Two configurations were tested, one with tail panels deflected 90° and one with tail panels deflected 70°. All the models were homogeneous and were machined from 4140 heat-treated steel. The center-of-gravity location for all the models was 3.4 d from the nose. The screw on the base of the 90°-panel model was used to secure the model to the sabot during launch. For the 70°-panel model the sweepback of the tail panels allowed alignment with the sabot, and so a screw was not used. The position of the center of gravity for all the models was measured within 0.0025 cm accuracy. The dimensions of the actual models varied only slightly from the nominal dimensions shown in figure 2. Nominal values of the measured physical characteristics of the models are listed in table I.

A photograph of the 90°-panel model with sabot is presented in figure 3. As can be seen, the sabot consisted of eight pieces; a four-piece nylon base used for transmitting the launching forces to the model, and four foam plastic fingers to help align the model in the gun. A hole drilled through the center of the nylon base allowed powder gases

inside to separate the sabot pieces from the model upon emerging from the gun muzzle. The plastic foam fingers were separated from the model upon emerging from the gun by the aerodynamic forces acting on the beveled front face. The sabots used to launch the 70°-panel models were nearly identical to the sabot shown in figure 3 except that the front face of the nylon base was beveled to fit the base of the model. The model was held in correct alignment with the sabot while being loaded into the gun by gluing the model to the sabot base. An adhesive which had little impact strength was used to enable the bond to break during the launch accelerations.

REDUCTION OF DATA

The data-reduction techniques used to deduce the aerodynamic coefficients of drag, lift, and static and dynamic stability from free-flight data obtained in the Ames Pressurized Ballistic Range are presented in reference 1. In this section it will be necessary to present only the basic equations used and a brief description of these techniques.

Drag

Drag coefficients were obtained directly from the flight time and distance measurements by the method presented in reference 2, which assumes a constant drag coefficient. The equation relating time and distance can be written (see ref. 1)

$$t = t_o - \frac{1}{V_o k C_D} + \frac{e^{kC_D x}}{V_o k C_D} \qquad (1)$$

where V_o and t_o are velocity and time at $x = 0$ and $k = \rho A/2m$. The parameters C_D, V_o, and t_o are determined which give the "best fit" to the measured values of x and t. A method applicable to cases where the drag coefficient varies with angle of attack is presented in reference 3. It is shown therein that if the drag coefficient varies with the resultant angle of attack according to the relation

$$C_D = C_{D_o} + C_{D_2}\sigma^2 \qquad (2)$$

then the effective drag coefficient obtained from equation (1) is the drag coefficient that would be obtained at a constant angle of attack equal to the root-mean-square resultant angle of attack of a given flight. The present results were found to be represented adequately by equation (2).

Static- and Dynamic-Stability Derivatives

The stability derivatives were determined from analysis of the pitching and yawing motions experienced by the models during free flight. The analysis consisted in fitting the following well-known tricyclic equation, derived in reference 4, to the measurements of α and β of each flight:

$$\beta + i\alpha = K_1 e^{(\eta_1 + i\omega_1)x} + K_2 e^{(\eta_2 - i\omega_2)x} + K_3 e^{ipx} \qquad (3)$$

where $\eta_{1,2}$ and $\omega_{1,2}$ are functions of the aerodynamic stability coefficients and $K_{1,2,3}$ are functions of the initial conditions. The most important assumptions inherent in this equation are linear aerodynamics, small angles of attack, constant roll rate, and small asymmetries. In the present analysis it was further assumed that the Magnus moment was zero. A least-squares procedure using differential corrections was used to determine optimum values of the constants.

The static- and dynamic-stability parameters are related to the constants in equation (3) as follows. The wavelength of the oscillation is given by

$$\lambda = \frac{2\pi}{\sqrt{\omega_1 \omega_2}} \qquad (4)$$

The quasi-linear pitching-moment-curve slope, C_{m_α}, is computed from the relation

$$C_{m_\alpha} = \frac{-8\pi^2 I_y}{\lambda^2 \rho A d} \qquad (5)$$

The dynamic-stability parameter, ξ, defined as

$$\xi = C_D - C_{L_\alpha} + \frac{md^2}{I_y}(C_{m_q} + C_{m_{\dot{\alpha}}}) \qquad (6)$$

is determined from the constants η_1 and η_2 by means of the relation

$$\xi = \frac{\eta_1 + \eta_2}{\rho A/2m} \tag{7}$$

It has been shown in references 5 and 6 that ξ is a measure of the dynamic stability of a vehicle both in unpowered flight at constant altitude and in ballistic entry.

RESULTS AND DISCUSSION

As stated earlier, the present investigation was primarily exploratory in nature, and therefore limited to determining the level of drag and static and dynamic stability of the two configurations at three Mach numbers, namely, 0.7, 1.5, and 3.5. A total of nine flights were obtained for analysis; one flight for each configuration at each Mach number, two additional flights at $M = 0.7$ for the 70°-panel model instrumented with small base pins to enable measurement of model roll rate, and one flight for the 70°-panel model launched backwards at $M = 0.7$. The measured values of C_D and C_{m_α} obtained from analysis of these flights are summarized in table II.

Shadowgraph Pictures

Shadowgraph pictures, typical of those obtained in the present tests, are presented in figures 4 through 7 for each configuration at each Mach number to [illegible] features of the flow field. The shadowgraphs are arrange[illegible] to Mach number in the following order:

Figs. 4(a)-4(d) - Shadowgraphs at M = 0.7

Figs. 5(a)-5(c) - Shadowgraphs at M = 1.5

Figs. 6(a)-6(d) - Shadowgraphs at M = 3.5

Figs. 7(a)-7(b) - Shadowgraphs of 70°-panel model launched backwards at M = 2.5

These shadowgraph pictures show a large turbulent flow-separation region which, in many instances, completely encompasses the tail panels. This separated-flow region effectively "slenderizes" the configuration; that is, it tends to make the body behave more like a slender cone, and therefore would be expected to significantly lower the drag and static stability of these configurations.* It can be seen that the separation point moves aft as the sweepback of the tail panels is increased from 90° to 70° (compare, for example, figs. 5(a) and 5(c)), and it moves forward for each configuration as the Mach number is increased (see figs. 5(a) and 6(a), also 5(c) and 6(c)). As the model pitches to larger angles of attack, the separated region becomes increasingly unsymmetrical (see, for example, fig. 5(b)), which would be expected to highly influence the variations of both static and dynamic stability of these configurations with angle of attack.

*As stated earlier, full-scale Reynolds numbers for these vehicles would be much higher than those obtained in the present tests. Any statement of how these higher Reynolds numbers would affect the flow about these models would be speculative.

Model Motions

The stability coefficients that will be presented are obtained from analysis of the oscillatory motions of models in free flight. One of the interesting results of the present tests was the model motions themselves. This is illustrated in figure 8, which shows the angular orientation histories of some of the flights. In this figure the angle of attack, α, is plotted versus the angle of sideslip, β; the circles show the measured data, and the lines are hand-fairings of these data. It can be seen that from about 2-1/2 to 4-1/2 cycles of model motion were obtained for these flights, and that about 5 to 8 values of α and β per cycle were obtained to define the motion. This number of cycles and data points per cycle is usually sufficient to obtain reliable aerodynamic coefficients. As indicated in figure 8, the motions obtained at Mach numbers of 1.5 and 3.5 were roughly similar in appearance. The motions are seen to be nearly planar with little roll, a type of motion frequently obtained in ballistic ranges. Conversely, some of the motions obtained at a Mach number of 0.7, particularly for the 70°-panel model, were very irregular (see figs. 8(c) through 8(f)). For these motions the character of each cycle is not repeated, high trim angles are indicated, and some of the excursions seem almost random. The reasons for these irregular motions are not known. Model damage should not be a cause since the models appear to have survived the much greater launching loads at the higher Mach numbers. It should be mentioned that the most irregular model motions were obtained with the two 70°-panel models

which were instrumented with base pins to enable measurements of model roll during the flight (flight nos. 1629 and 1630, see figs. 8(e) and 8(f), also fig. 4(d)). However, this apparent correlation is believed to be fortuitous since these small base pins had an insignificant effect on model center of gravity, weight, moments of inertia, etc., and therefore should not have had any effect on the model motions.

As discussed in the section entitled "Reduction of Data," theoretical motions are obtained by fitting equation (3) to the experimental α,β data. The closeness of the theoretical motions to the experimental data is a measure of the reliability of the stability results. The fitted curves for all the flights analyzed in the present investigation gave standard deviations that were from about 2 to 10 times greater than the stated measuring accuracy, 0.25°. It is believed that the large unsteady separated flow region about these models so highly influenced the motions that equation (3) was not practicably applicable. In addition it is recognized that these configurations are not axisymmetric and therefore the stability coefficients are a function of roll angle. This is another reason why equation (3) is not strictly applicable. Although the model motions indicate that the roll rates for these flights were not large (the measured roll rates for flight nos. 1629 and 1630 were from about 0.6°/ft for the initial portion of the flights to about 1.5°/ft towards the end of the flights), this amount of roll and/or roll acceleration could have a significant effect on the motions of this type of configuration.

Drag Characteristics

As stated earlier, a summary of the aerodynamic data obtained in the present investigation is given in table II. The measured values of drag coefficient at zero degrees angle of attack are presented as a function of Mach number in figure 9. The data presented near a Mach number of 1.5 were obtained from a single flight of each configuration; that is, each flight was broken up into three portions and each portion was analyzed independently to give three data points for each configuration. For most of the flights a short straight-line extrapolation of the drag data, that is, C_D plotted versus the root-mean-square resultant angle of attack, was made to obtain the drag coefficients at $\alpha = 0°$. The experimental data show that changing the sweepback angle of the tail panels from 90° to 70° had little effect on the drag coefficients throughout the Mach number range investigated. Also, the drag coefficient decreases by about 40 percent as the Mach number is increased from 1.5 to 3.5. Theoretical estimates, at $M = 20$, and empirical estimates at the lower Mach numbers (ref. 7) are also presented in figure 9.† However, because of the inability of these prediction techniques to account for the effect on drag coefficient of the large separated-flow region which exists over these models (as discussed previously), it is not expected that good agreement would be obtained.

†The estimates shown at the subsonic, transonic, and supersonic Mach numbers were obtained using the ratio of panel to cylinder cross-sectional area and the experimental data from reference 8; the hypersonic estimates were obtained from the computer program of reference 9.

As shown in figure 9, these estimates badly overpredict (by about 100 percent) the drag coefficients at a Mach number of 3.5 and show a decrease in drag coefficient of about 17 percent for a change in tail panel sweepback angle from 90° to 70°. The agreements between the experimental data and the estimates for either configuration at Mach numbers of 0.7 and 1.5 are thus likely to be purely fortuitous.

Static Stability Characteristics

The experimental static stability data are presented in figure 10, where values of the quasi-linear pitching-moment-curve slope, C_{m_α}, are plotted as a function of Mach number. Although the angle-of-attack range of most of these flights was small (usually below 10°, see table II), important nonlinear effects could be present in the data due to the changing influence of the separated-flow region on the tail panels. As stated previously, with the exception of the 70°-panel model at a Mach number of 0.7, only one flight of each configuration at each Mach number was obtained; therefore, the variation of C_{m_α} with angle of attack could not be adequately ascertained with these limited data. The values of C_{m_α} presented in figure 10 correspond to average values of an equivalent linear system which best fit the measured angular orientation data of each flight. The data presented in figure 10 are for a common center-of-gravity position, 3.4 d from the nose.

In order to investigate the sensitivity of C_{m_α} to changes in various factors such as roll rate, angle of attack, and Mach number, the present flights were broken up into 1-1/2 cycle portions and these

portions were analyzed separately. These portions were also analyzed using various assumed values of roll rate to determine the effect of roll rate on C_{m_α}. It was found that for each flight the values of C_{m_α} varied by only about 10 to 20 percent; therefore values of C_{m_α} presented herein are average values determined from the above procedure. Analys of these flights using more sophisticated, less restrictive, data-reduction techniques could have been accomplished; however, this would entail considerable additional effort which for the present exploratory investigation was considered unwarranted.

The data shown in figure 10 show that both configurations are statically stable throughout the Mach number range investigated and that changing the sweepback angle of the tail panels from 90° to 70° has little effect on the static stability. A high degree of sensitivity of the static stability to small changes in Mach number is apparent at the subsonic and transonic Mach numbers. The theoretical estimate of static stability at a Mach number of 20 (ref. 7) is seen to be much lower than the experimental data obtained for the Mach number range of the present investigation.

As stated earlier, one flight was made using a 70°-panel model launched backwards (180° orientation) at a Mach number of about 2.5. The angular orientation - distance history of this flight is presented in figure 11. As can be seen, the model remained flying backwards for about 12 meters (40 feet), which indicates a nearly disturbance-free separation of the model from its sabot upon emerging from the gun, then started to turn around. During the remainder of the flight the model passed through

the nose-forward attitude ($\alpha = 0°$), continued to an angle of pitch (and yaw) of about 120°, and then began to return towards a nose-forward attitude when it impacted the catcher after 62 m (203 feet) of flight. This flight indicates that no stable trim point exists at an angle of attack of 180° (backwards orientation) for this configuration at these test conditions.

Dynamic Stability Characteristics

The dynamic behavior of these configurations was found to be erratic, a not unexpected result considering the separated flow (figs. 4-7) and the irregular model motions presented in figure 8. The dynamic stability appears to be a function of Mach number, angle of attack, and roll rate, and for this reason values of ξ and/or $C_{m_q} + C_{m_{\dot{\alpha}}}$ are not given as they would be misleading. A qualitative discussion of the dynamic behavior of each flight is included in table II. As can be seen, the configurations exhibited essentially neutral dynamic stability in four of the flights and dynamic instability in the remaining four flights. As noted in table II, flight no. 1625 demonstrated a high degree of dynamic instability. It should be mentioned in relation to this flight that small particles of the plastic foam sabot fingers may have adhered to the front surfaces of some of the tail panels (see figs. 4(b) and (c)). However, it is hard to believe that the presence of these small plastic foam particles would be sufficient to cause the large dynamic instability noted for this flight.

CONCLUDING REMARKS

The following remarks summarize the results of this exploratory investigation. The tests were conducted in a ballistic range to determine the drag and static and dynamic stability of a proposed space shuttle booster vehicle at Mach numbers of 0.7, 1.5, and 3.5. Two configurations were tested, one with tail panels deflected 90° and one with tail panels deflected 70°.

1. The change in sweepback angle of the tail panels had little effect on the drag and static and dynamic stability of the vehicle at all Mach numbers investigated.

2. The drag coefficients of both configurations decrease by about 40 percent as the Mach number is increased from 1.5 to 3.5. Empirical estimates, and also theoretical estimates at a Mach number of 20, overpredict by about 100 percent the drag coefficients obtained at a Mach number of 3.5, and also predict a decrease of about 17 percent in drag coefficient for a change in sweepback angle of the tail panels from 90° to 70°.

3. The flow field over the models is characterized by an extensive separated-flow region which largely encompasses the tail panels of both configurations at all Mach numbers investigated. This separated flow undoubtedly influences the drag and static- and dynamic-stability characteristics of the configurations and, as a consequence, also influences the motions experienced by the models during free flight.

4. The model motions, in particular those obtained at a Mach number of 0.7, were very irregular and could not be fitted accurately by standard quasi-linear data-reduction techniques to extract static- and dynamic-stability coefficients.

5. The present experimental static-stability results are believed accurate only to about 10 to 20 percent, but clearly show that both configurations are statically stable at all Mach numbers investigated. Theoretical estimates of the static stability for the 90°-panel model at a Mach number of 20 was much lower than the present experimental results.

6. The dynamic behavior of both configurations was very erratic; four of the flights indicated essentially neutral dynamic stability, and the remaining four flights indicated dynamic instability.

7. The results of one flight of a 70°-panel model, launched backwards at a Mach number of 2.5, indicated that no stable trim point exists at this $\alpha = 180°$ orientation at these test conditions.

REFERENCES

1. Malcolm, G. N.; and Chapman, G. T.: A Computer Program for Systematically Analyzing Free-Flight Data to Determine the Aerodynamics of Axisymmetric Bodies. NASA TN D-4766, 1968.

2. Seiff, A.: A New Method for Computing Drag Coefficients from Ballistic Range Data. J. Aerosp. Sci., vol. 25, no. 2, 1958, pp. 133-134.

3. Seiff, A.; and Wilkins, M. E.: Experimental Investigation of a Hypersonic Glider Configuration at a Mach Number of 6 and at Full-Scale Reynolds Numbers. NASA TN D-341, 1961.

4. Nicolaides, J. D.: On the Free-Flight Motion of Missiles Having Slight Configurational Asymmetries. Rep. No. 858, Ballistic Research Laboratories, 1953.

5. Seiff, A.; Sommer, S. C.; and Canning, T. N.: Some Experiments at High Supersonic Speeds on the Aerodynamic and Boundary-Layer Transition of High-Drag Bodies of Revolution. NACA RM A56I05, 1957.

6. Allen, H. J.: Motion of a Ballistic Missile Angularly Misaligned with the Flight Path upon Entering the Atmosphere, and Its Effect upon Aerodynamic Heating, Aerodynamic Loads, and Miss Distance. NACA TN 4048, 1957.

7. Graham, R. E.: Private Communication, NASA Manned Spacecraft Center, December 9, 1971, and January 5, 1972.

8. Regan, F. J.: The Aerodynamic Characteristics of an Ogive Cylinder with Split-Skirt Stabilizer at Subsonic, Transonic, and Supersonic Speeds. Rep. no. NOL TR 63-86, U. S. Naval Ordnance Lab., 1966.

9. Anon: Hypersonic Arbitrary-Body Aerodynamic Computer Program (Mark III Version). Rep. no. 61552, Douglas Aircraft Corp., 1968.

TABLE I.- NOMINAL VALUES OF MODEL PHYSICAL CHARACTERISTICS

	90°-panel model	70°-panel model
d (cylinder dia)	1.78 cm (0.7 in.)	1.78 cm
Model mass	208 gm	206 gm
x_{cg}/d (from nose)	3.4	3.4
I_y, I_z	19.6×10^{-5} kg-m^2 (14.5×10^{-5} slug-ft^2)	19.6×10^{-5} kg-m^2
I_x	1.1×10^{-5} kg-m^2 (0.84×10^{-5} slug-ft^2)	1.1×10^{-5} kg-m^2

TABLE II.- SUMMARY OF TEST RESULTS

Flight no.	Deflection angle of tail panels, deg	Mach no.	Reynolds no. (based on d), million	C_{D_o}	C_{m_α}, 1/rad	Dynamic behavior
1622	90	0.7	0.30	5.4	-7.	Amplitude of motion stays about constant (1°).
1625	70	.7	.30	5.0	-9.	Amplitude grows significantly with distance flown, from 2° to about 15°.
1629	70	.5	.22	4.7	-5.	Amplitude stays about constant (3.5°).
1630	70	.7	.30	5.0	-7.	Amplitude stays about constant (1.5°).
1614	90	1.6	.68	5.0	-13.	Amplitude increases from 4° to 6°.
		1.5	.63	5.2	-18.	
		1.4	.59	5.5	-20.	
1624	70	1.6	.68	5.1	-13.	Amplitude stays about constant (2°).
		1.5	.63	5.4	-17.	
		1.4	.59	5.6	-22.	
1623	90	3.5	1.48	3.1	-17.	Amplitude increases from 6° to 8°.
1626	70	3.5	1.46	3.0	-17.	Amplitude increases from about 10° to 12° and then appears to adopt a limit cycle behavior.
1628	70	2.5	Model launched backwards			

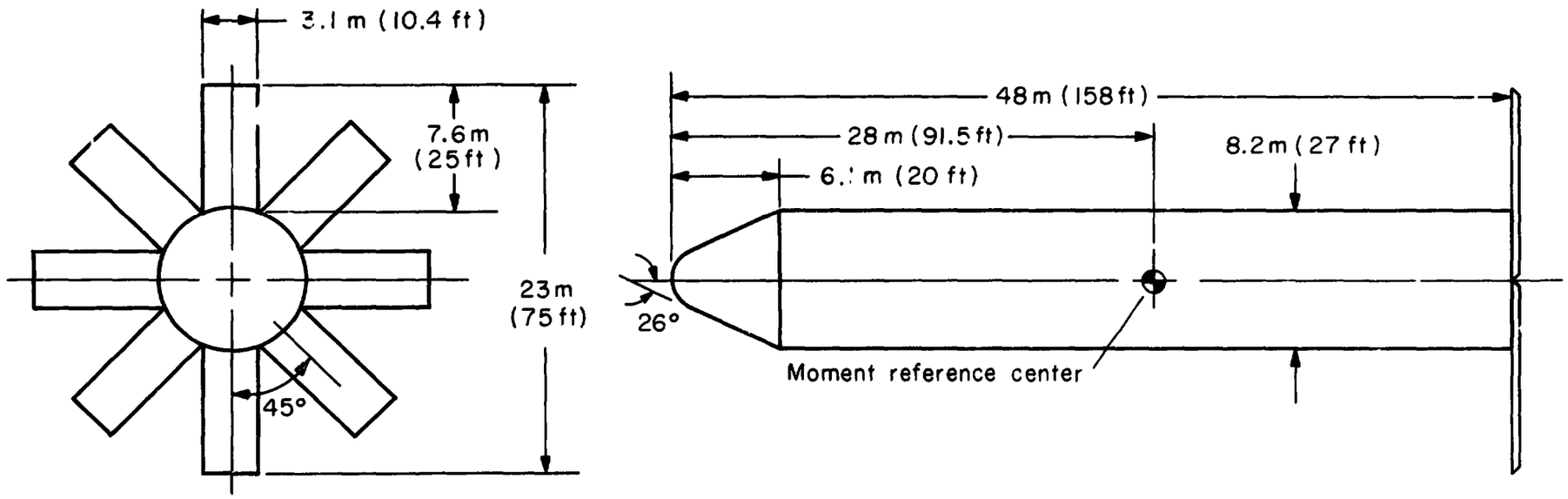

Figure 1.- Sketch of proposed booster giving nominal full-scale dimensions.

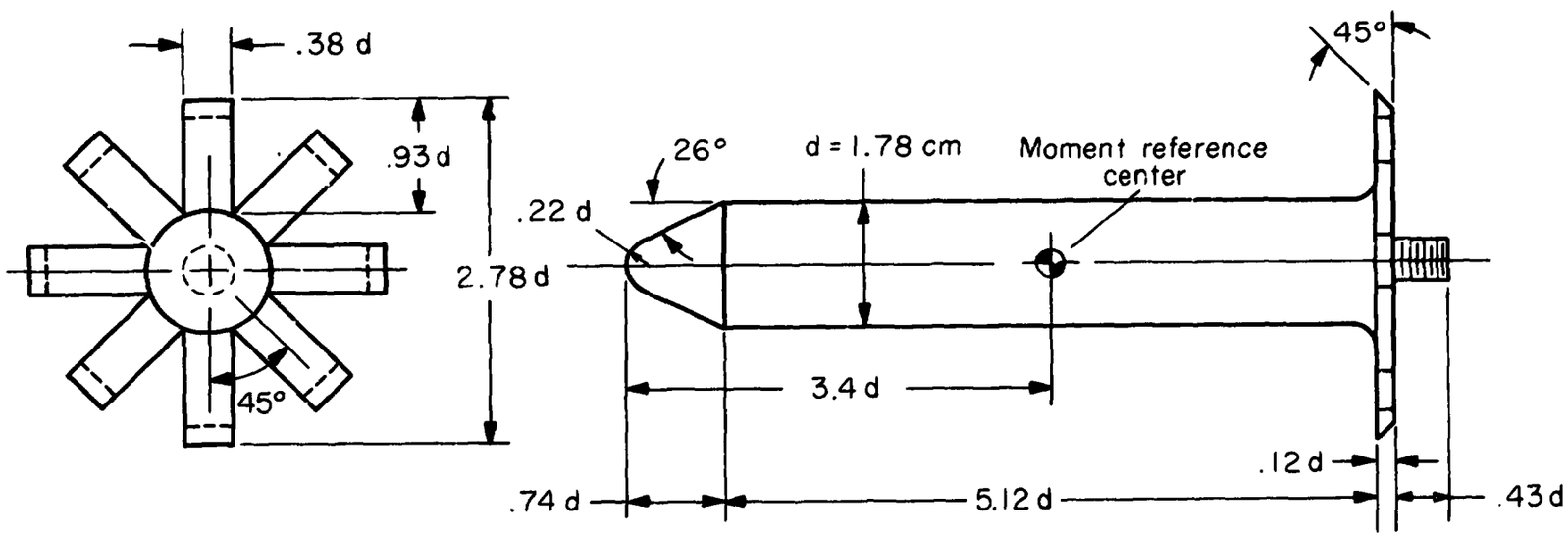

(a) Model with tail panels deflected 90°.

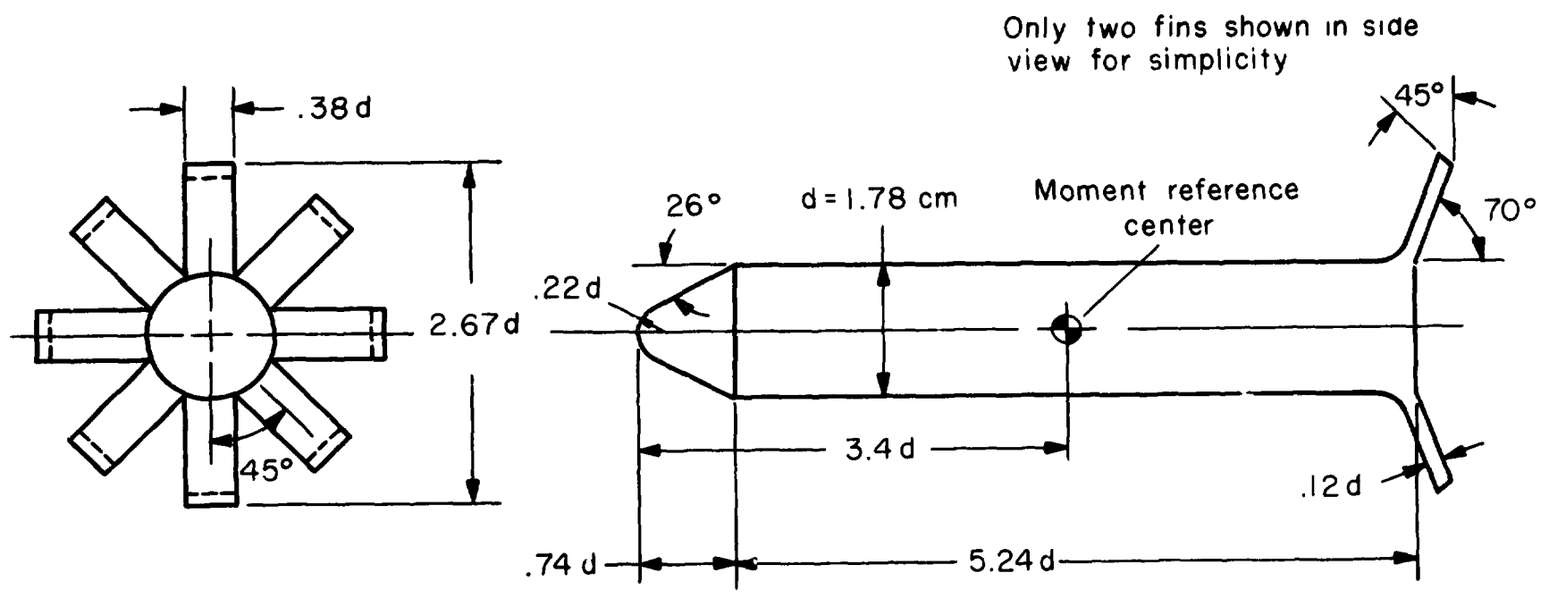

(b) Model with tail panels deflected 70°.

Figure 2.- Sketches of models showing nominal dimensions.

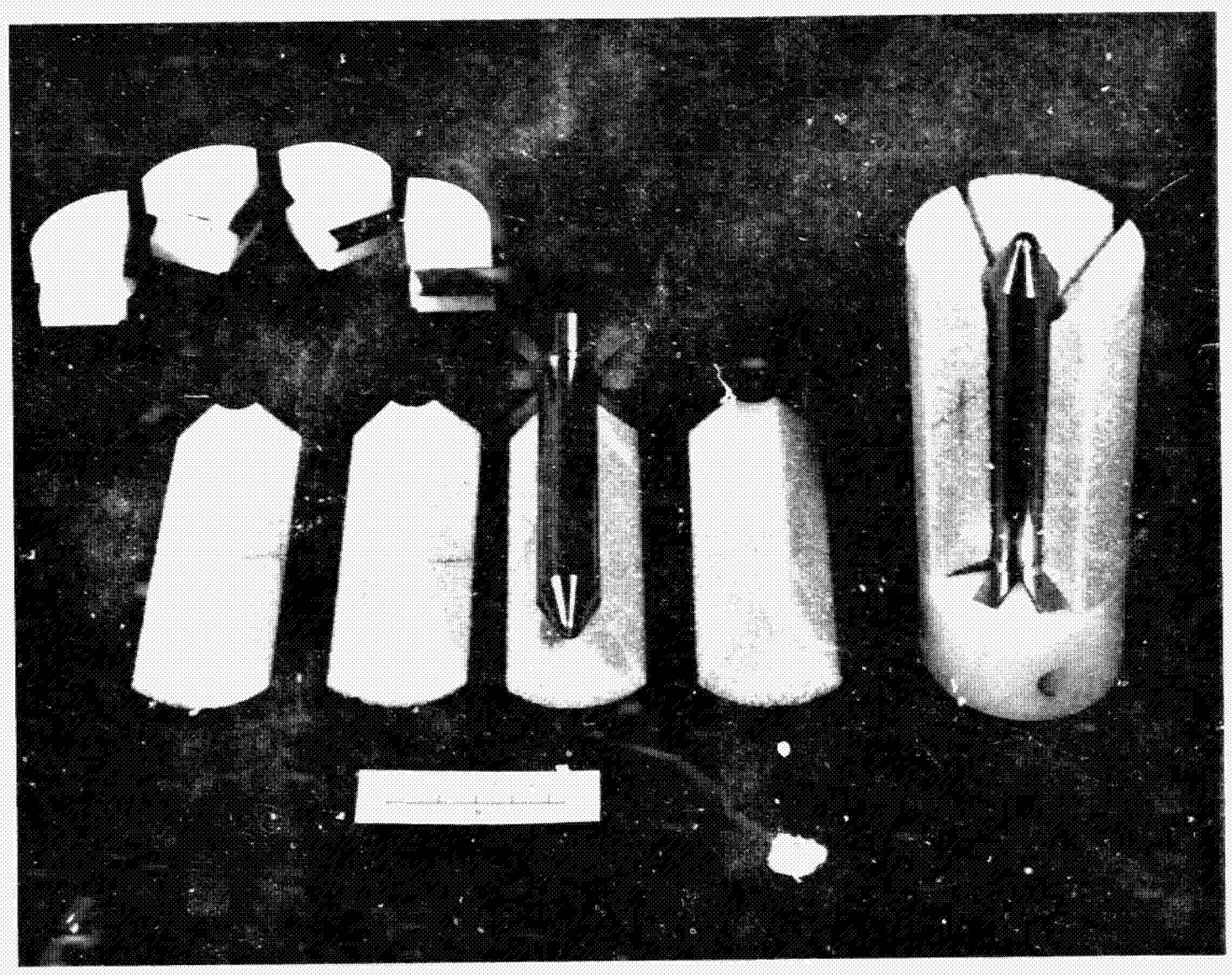

Figure 3.- Photograph of 90°-panel model and sabot.

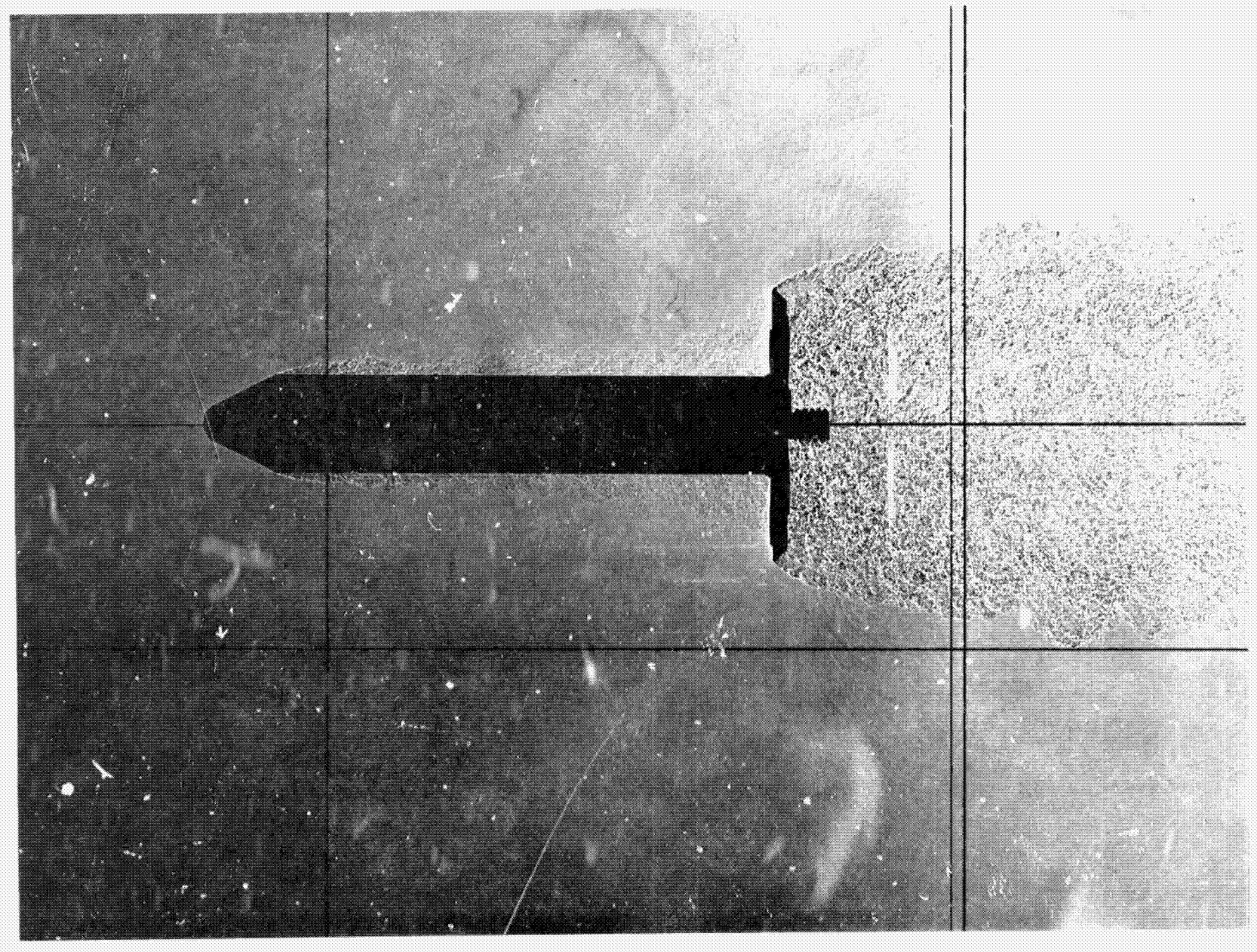

(a) 90°-panel model, M = 0.7, flight no. 1622, $\alpha = 0.25°$, ($\beta = -0.65°$).

Figure 4.- Typical shadowgraphs of models in flight at a Mach number of 0.7.

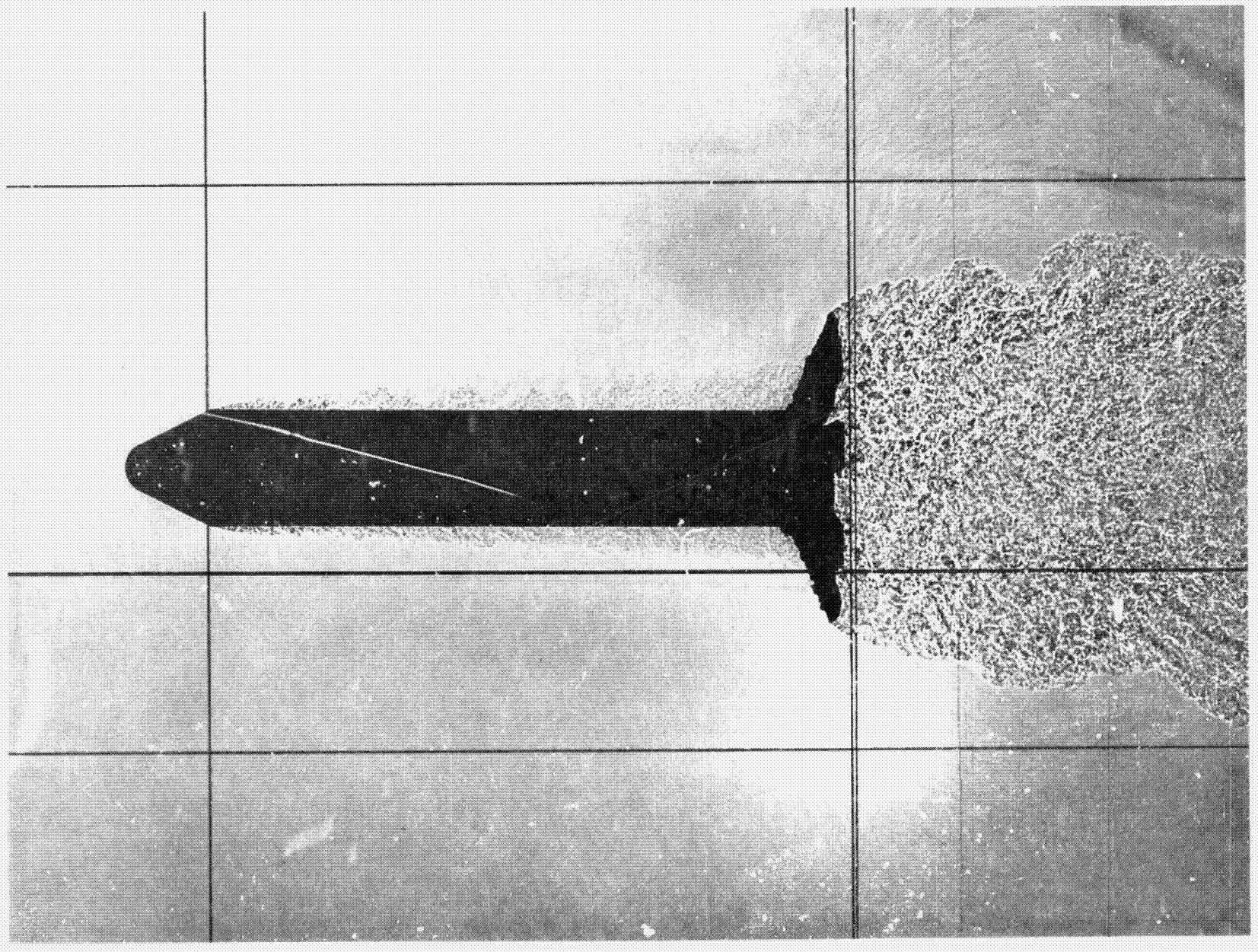

(b) 70°-panel model, M = 0.7, flight no. 1625, α = 0.45°, (β = -2.17°).

Figure 4.- Continued.

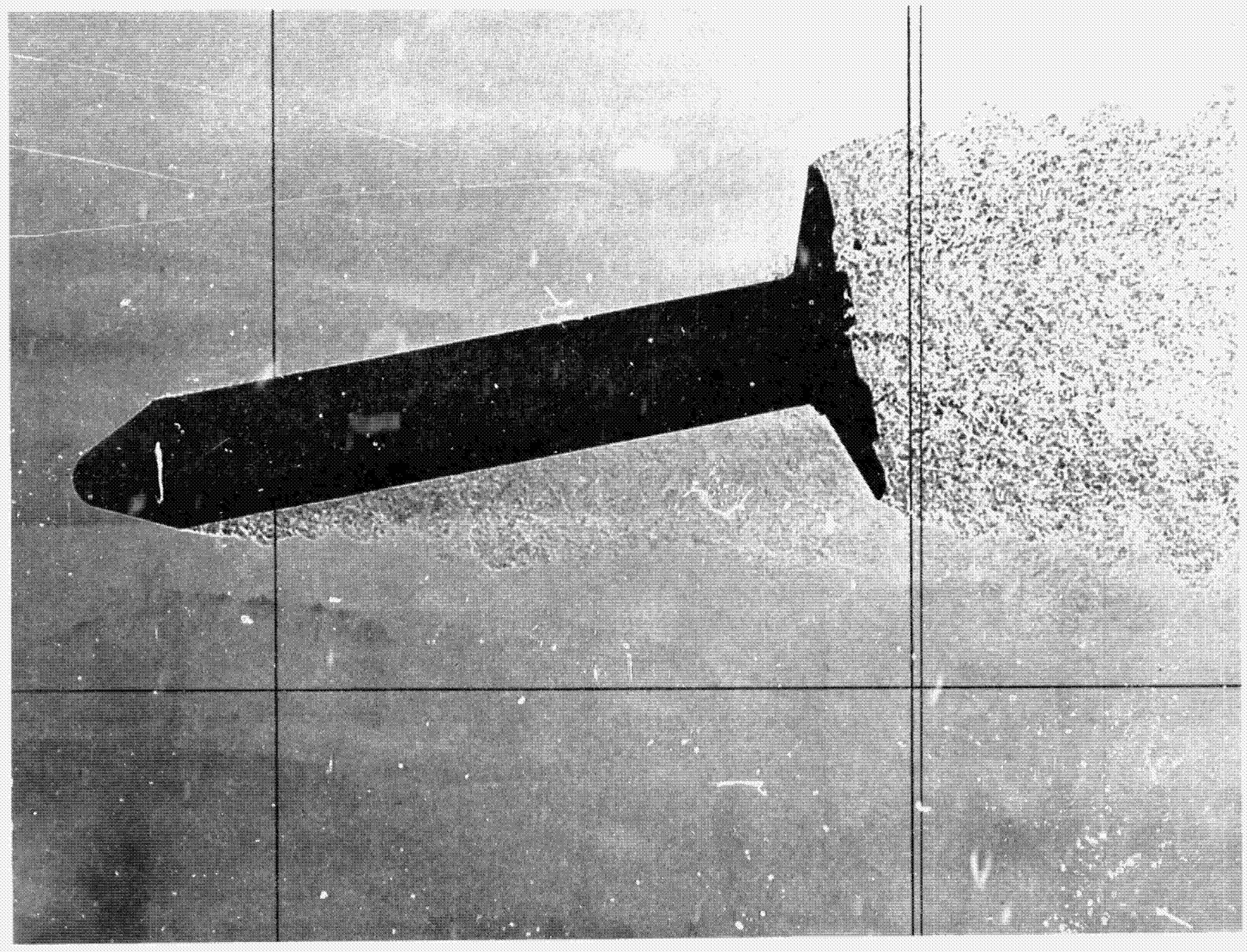

(c) 70°-panel model, M = 0.7, flight no. 1625, $\alpha = -10.77°$, ($\beta = -2.80°$).

Figure 4.- Continued.

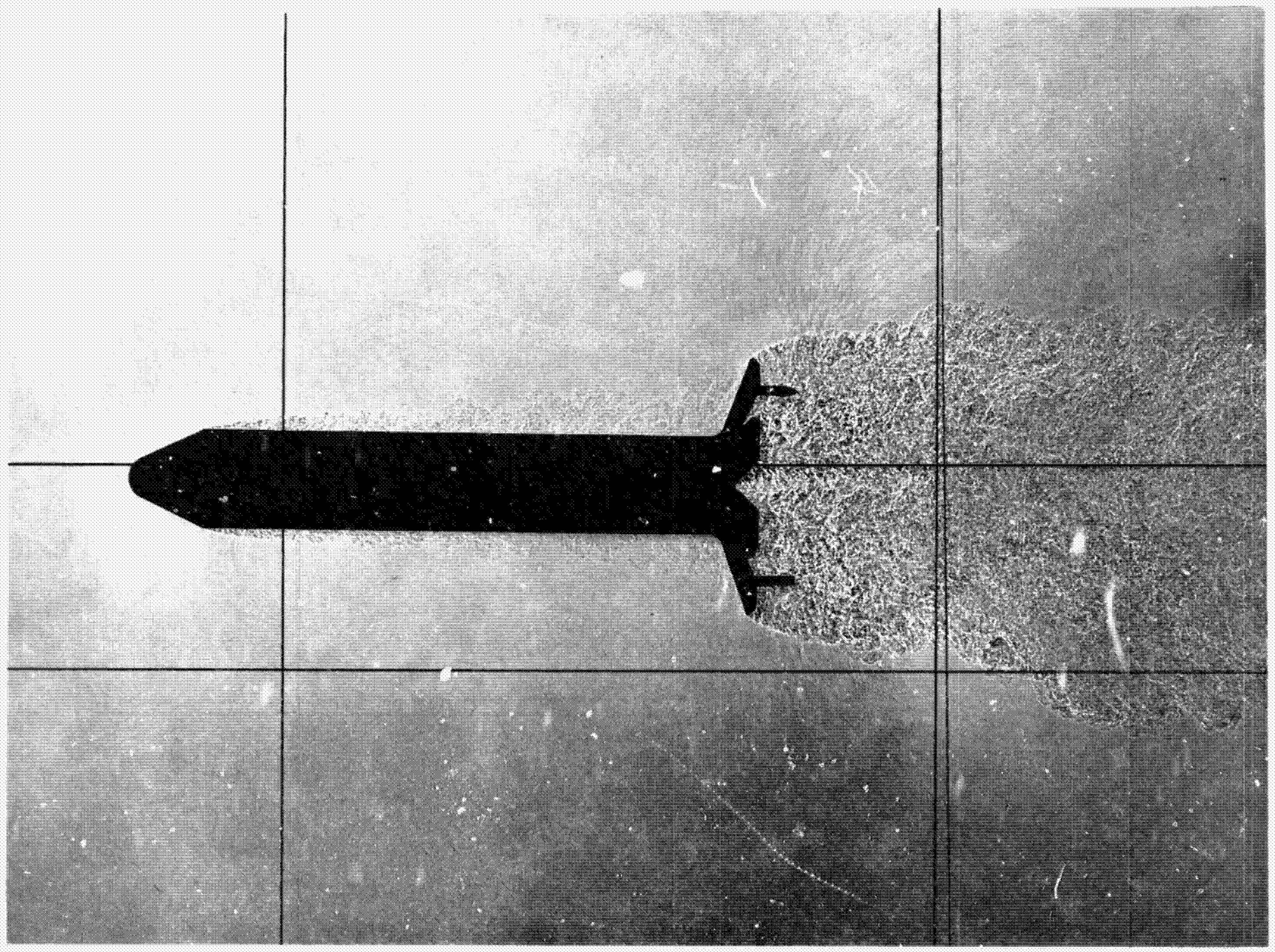

(d) 70°-panel model with base pins, M = 0.7, flight no. 1630, α = 0.68°, (β = 0.80°).

Figure 4.- Concluded.

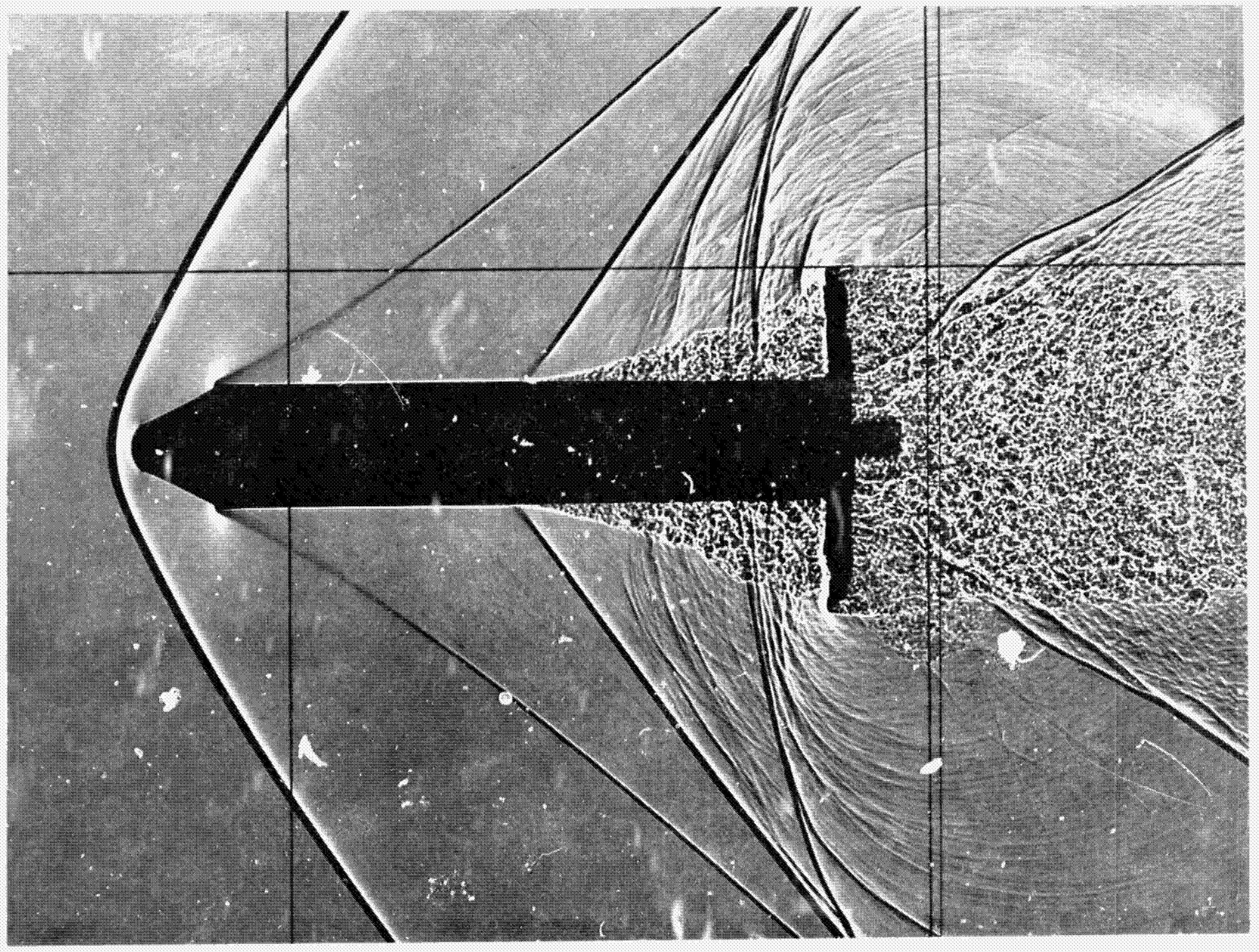

(a) 90°-panel model, M = 1.5, flight no. 1614, α = -0.36°, (β = -2.70°).

Figure 5.- Typical shadowgraphs of models in flight at a Mach number of 1.5.

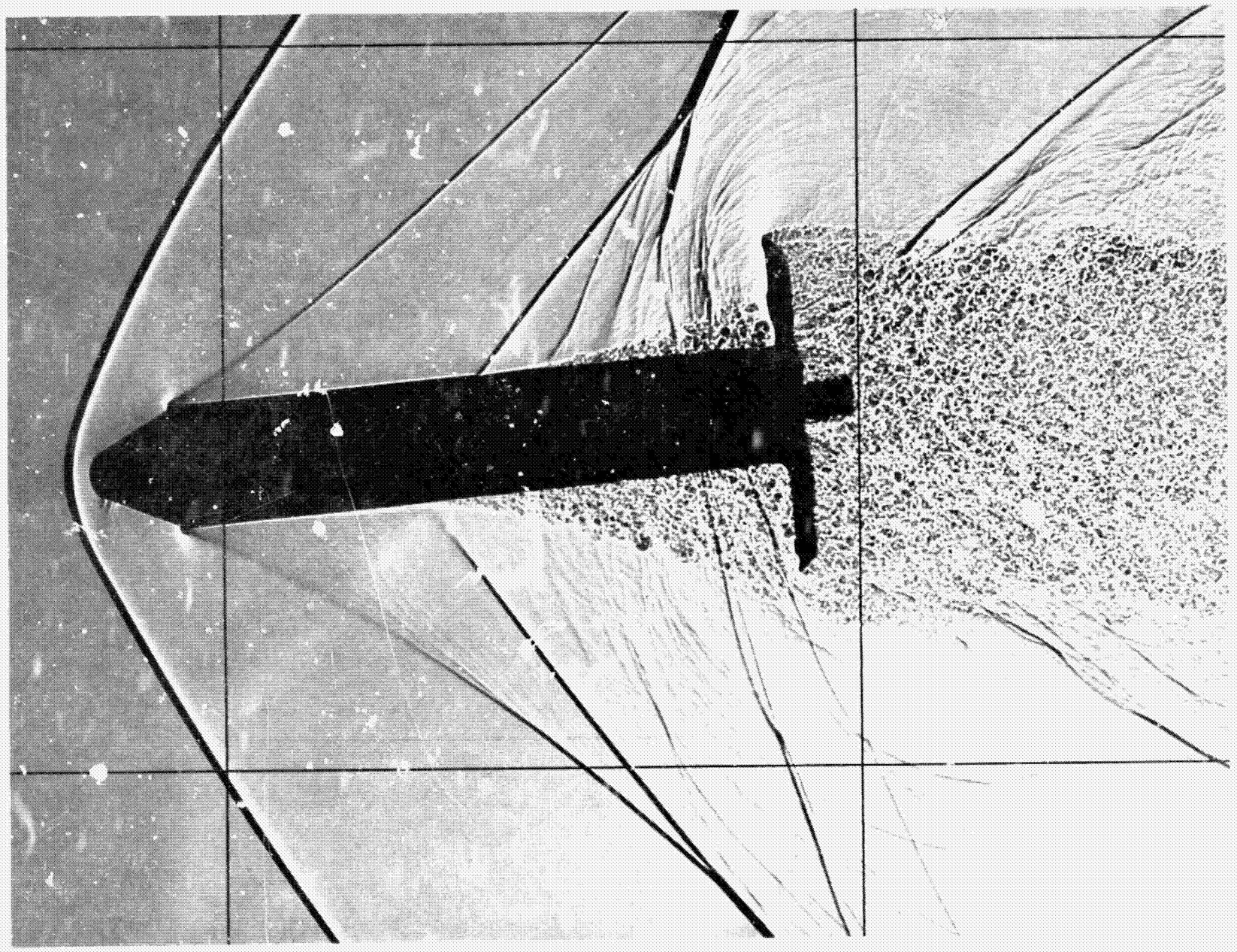

(b) 90°-panel model, M = 1.5, flight no. 1614, β = 5.65°, (α = 2.43°).

Figure 5.- Continued.

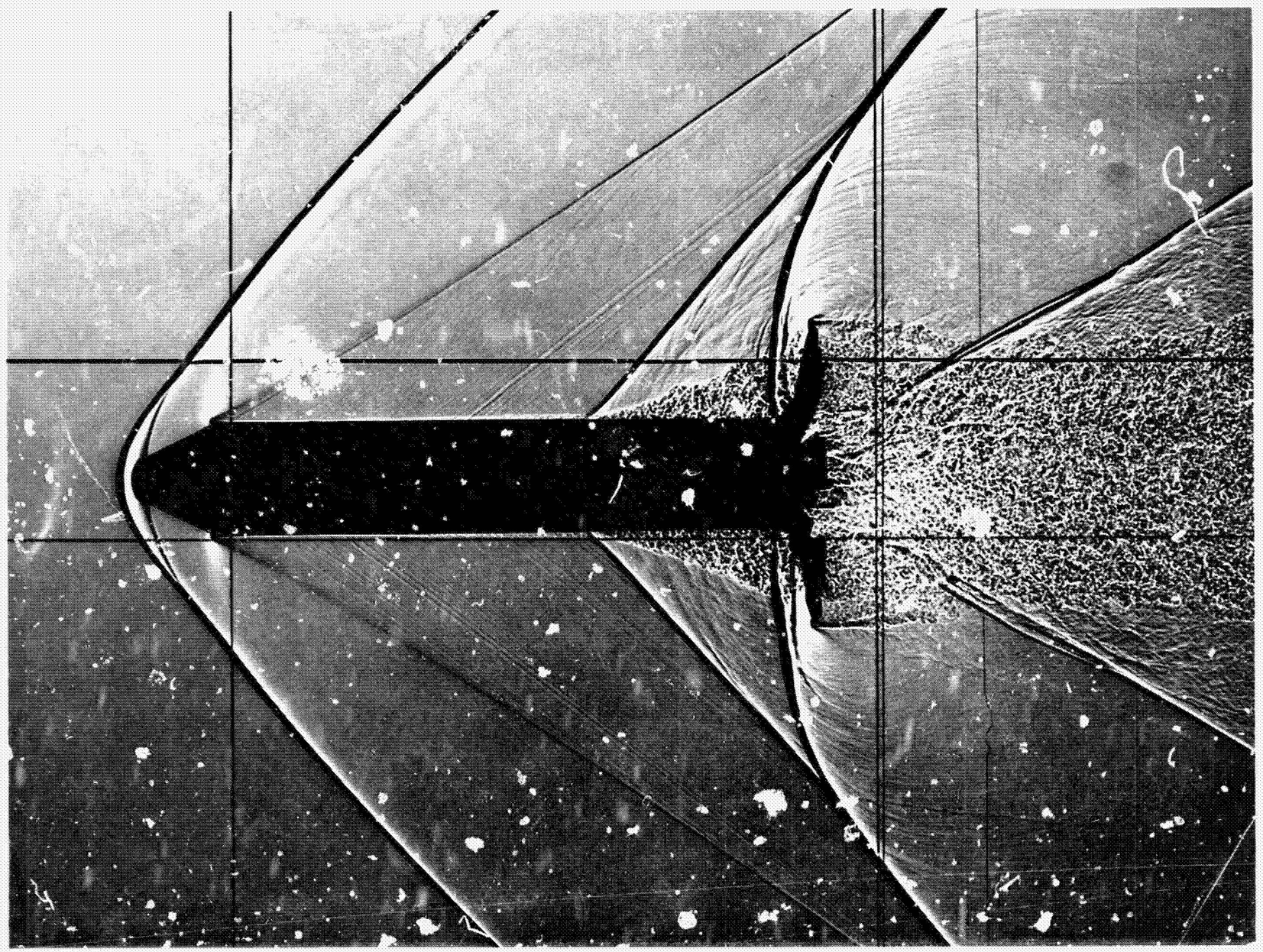

(c) 70°-panel model, M = 1.5, flight no. 1624, $\alpha = -0.65°$, ($\beta = 2.19°$)

Figure 5.- Concluded.

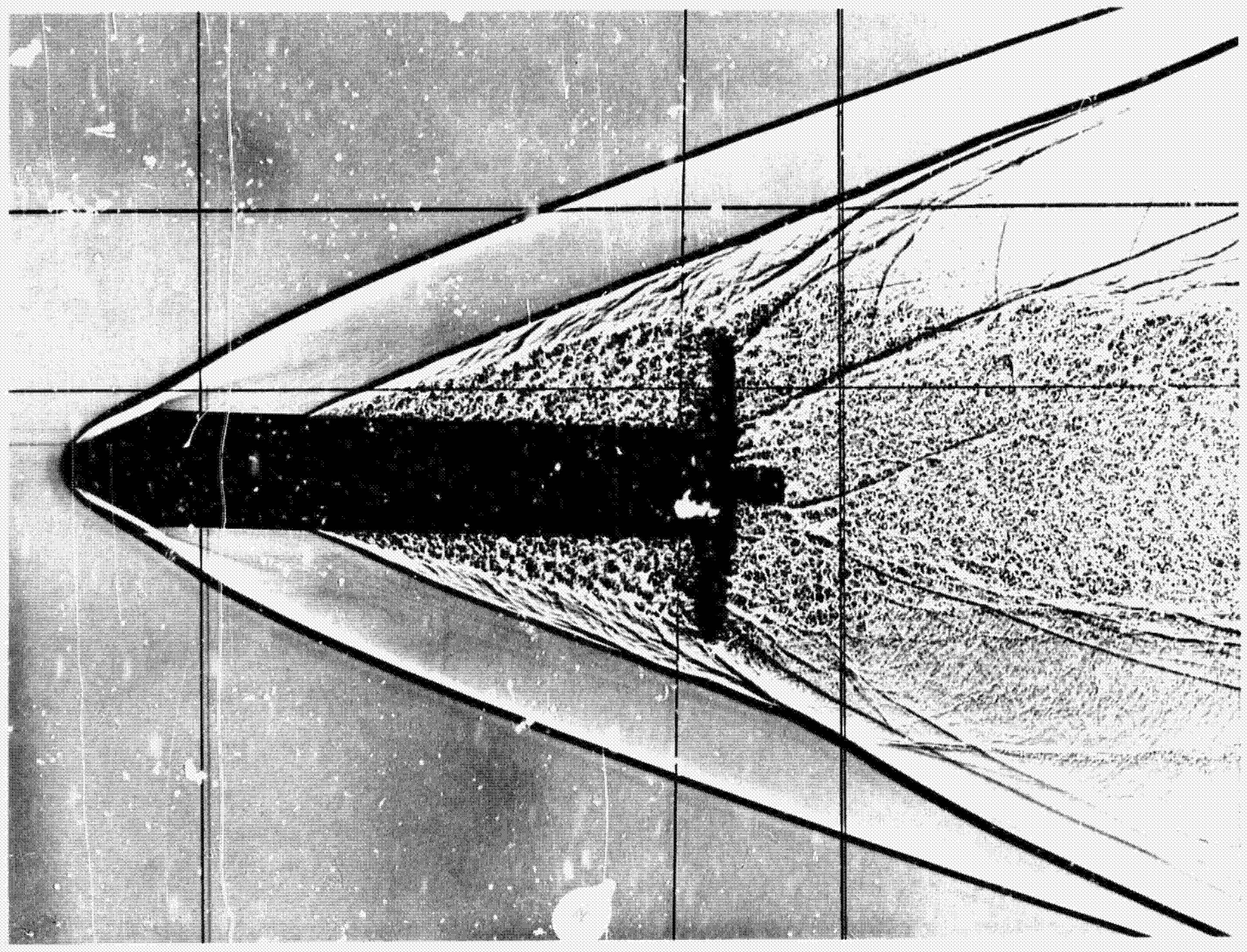

(a) 90°-panel model, M = 3.5, flight no. 1623, α = 1.91°, (β - 3.52°).

Figure 6.- Typical shadowgraphs of models in flight at a Mach number of 3.5.

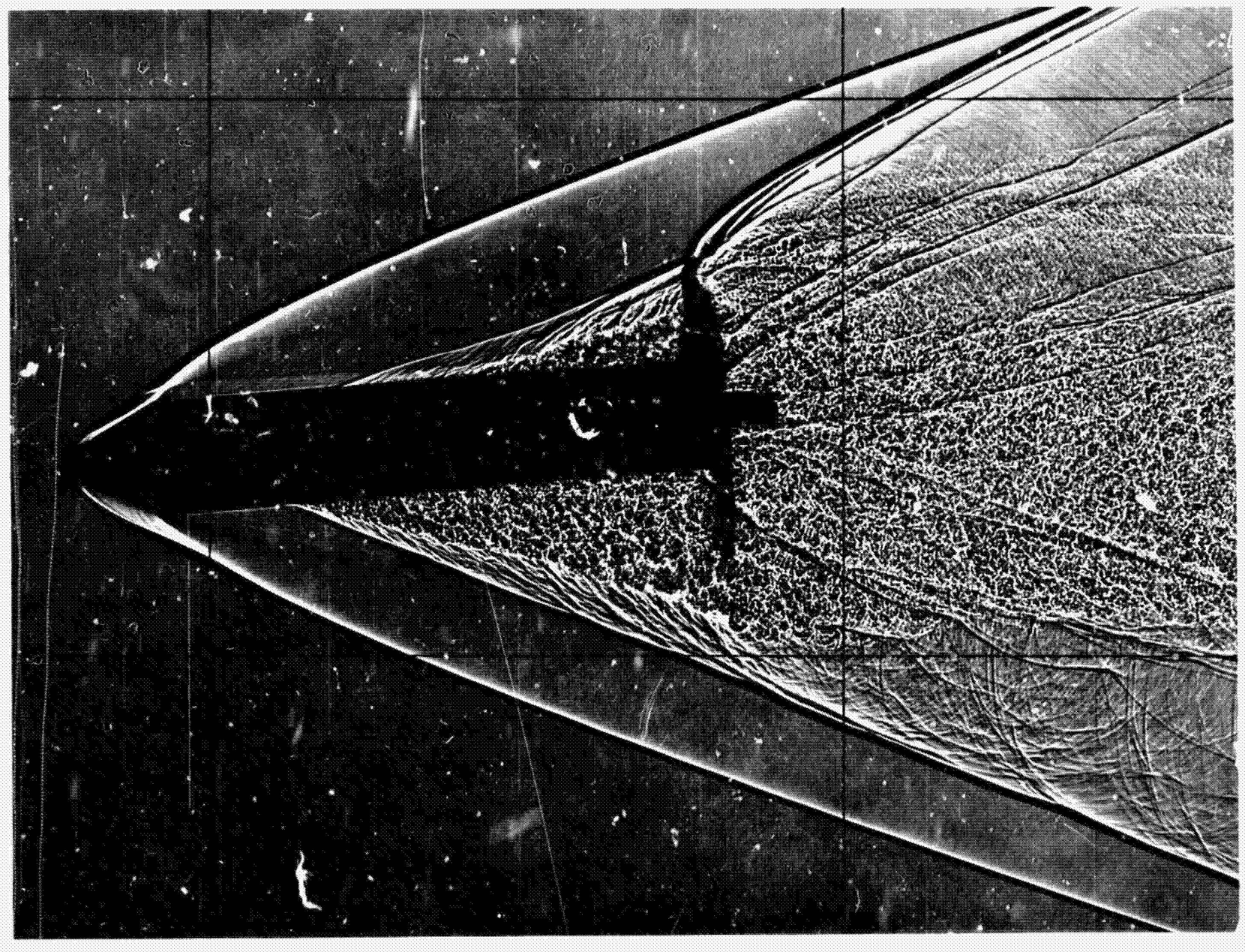

(b) 90°-panel model, M = 3.5, flight no. 1623, $\beta = 4.65°$, ($\alpha = 3.06°$).

Figure 6.- Continued.

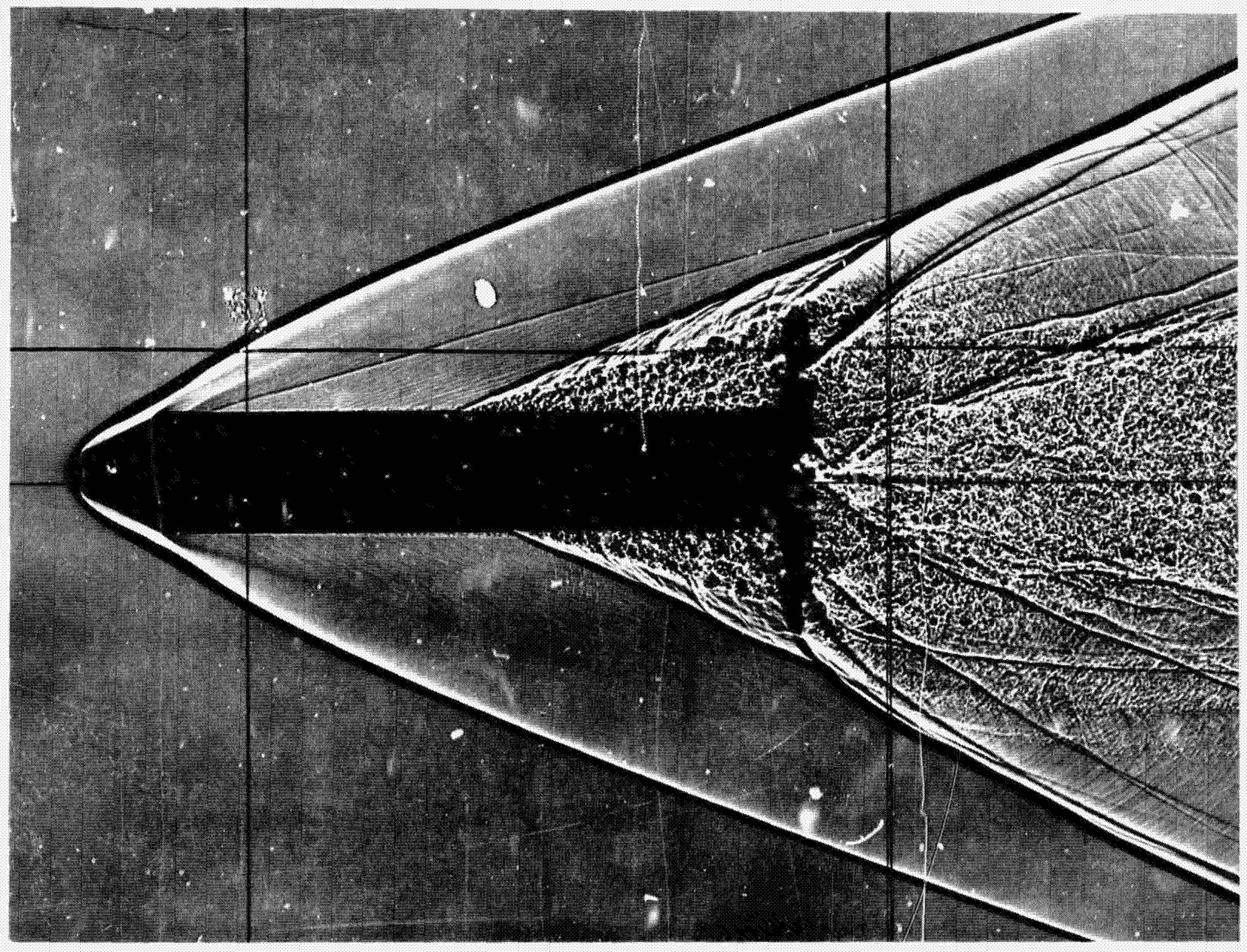

(c) 70°-panel model, M = 3.5, flight no. 1626, $\alpha = -0.29°$, ($\beta = -0.56°$).

Figure 6.- Continued.

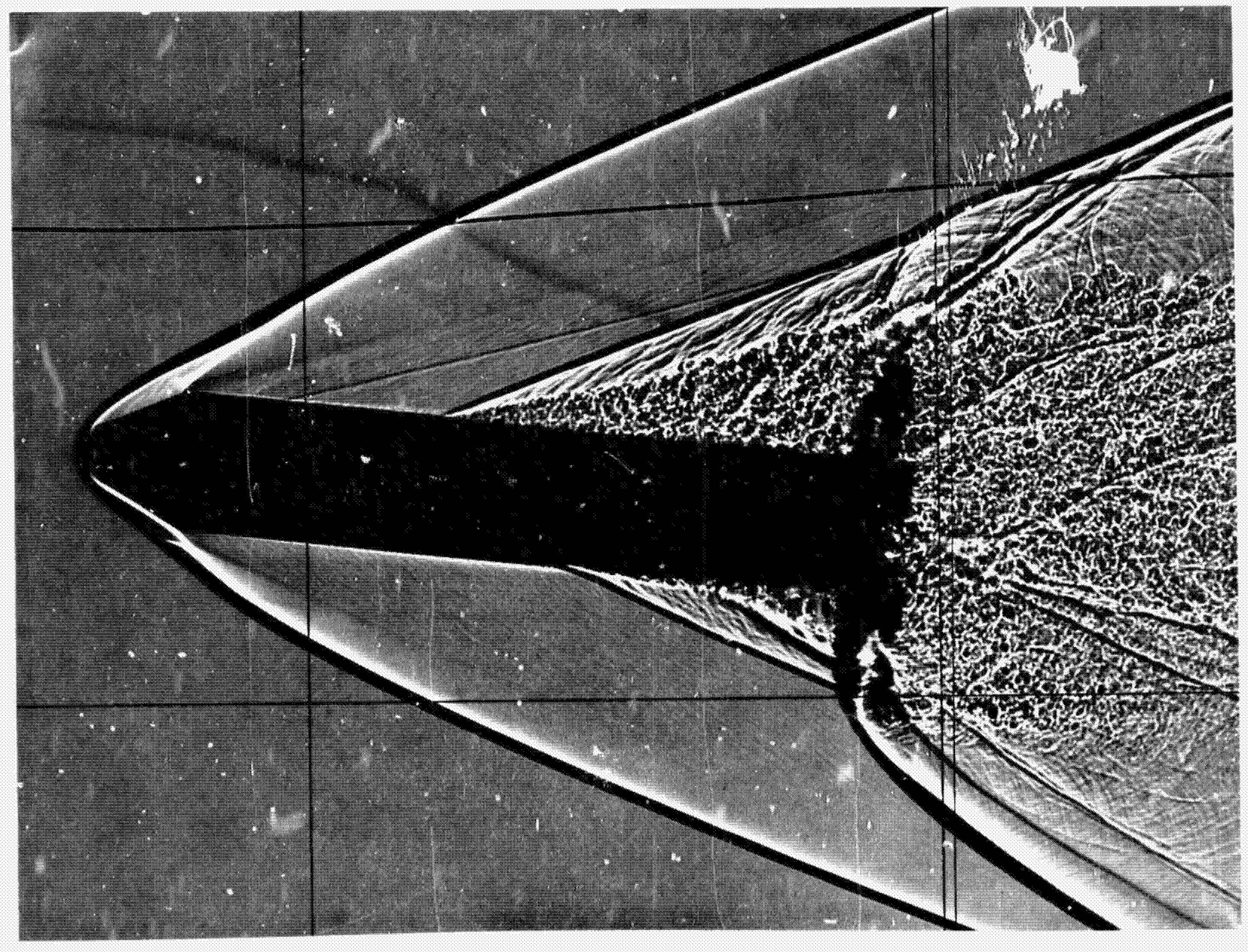

(d) 70°-panel model, M = 3.5, flight no. 1626, α = 6.02°, (β = -5.58°).

Figure 6.- Concluded.

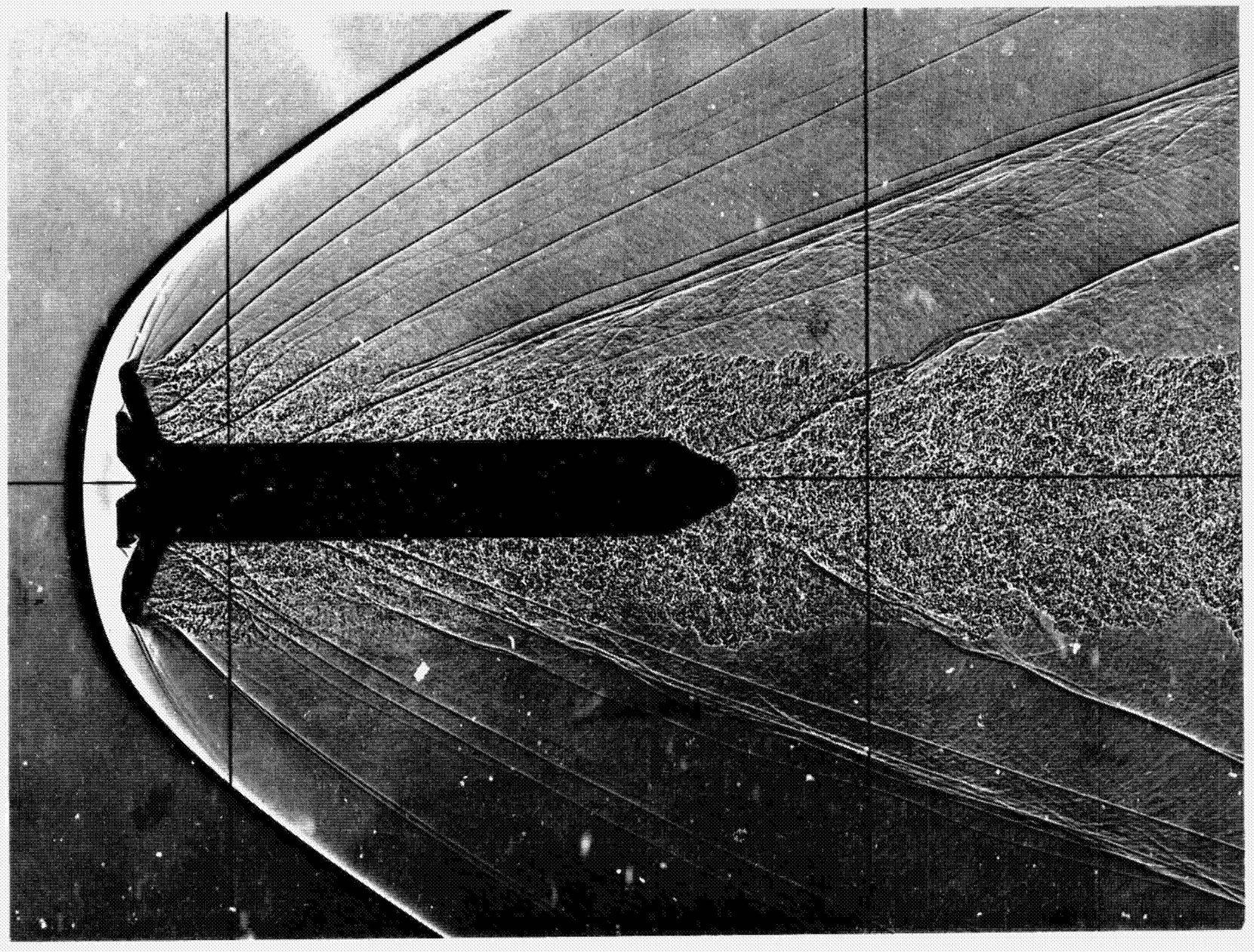

(a) 70°-panel model, M = 2.5, flight no. 1628, β = 180.4°, (α = 180 0°).

Figure 7.- Shadowgraphs of model launched backwards at a Mach number of 2.5.

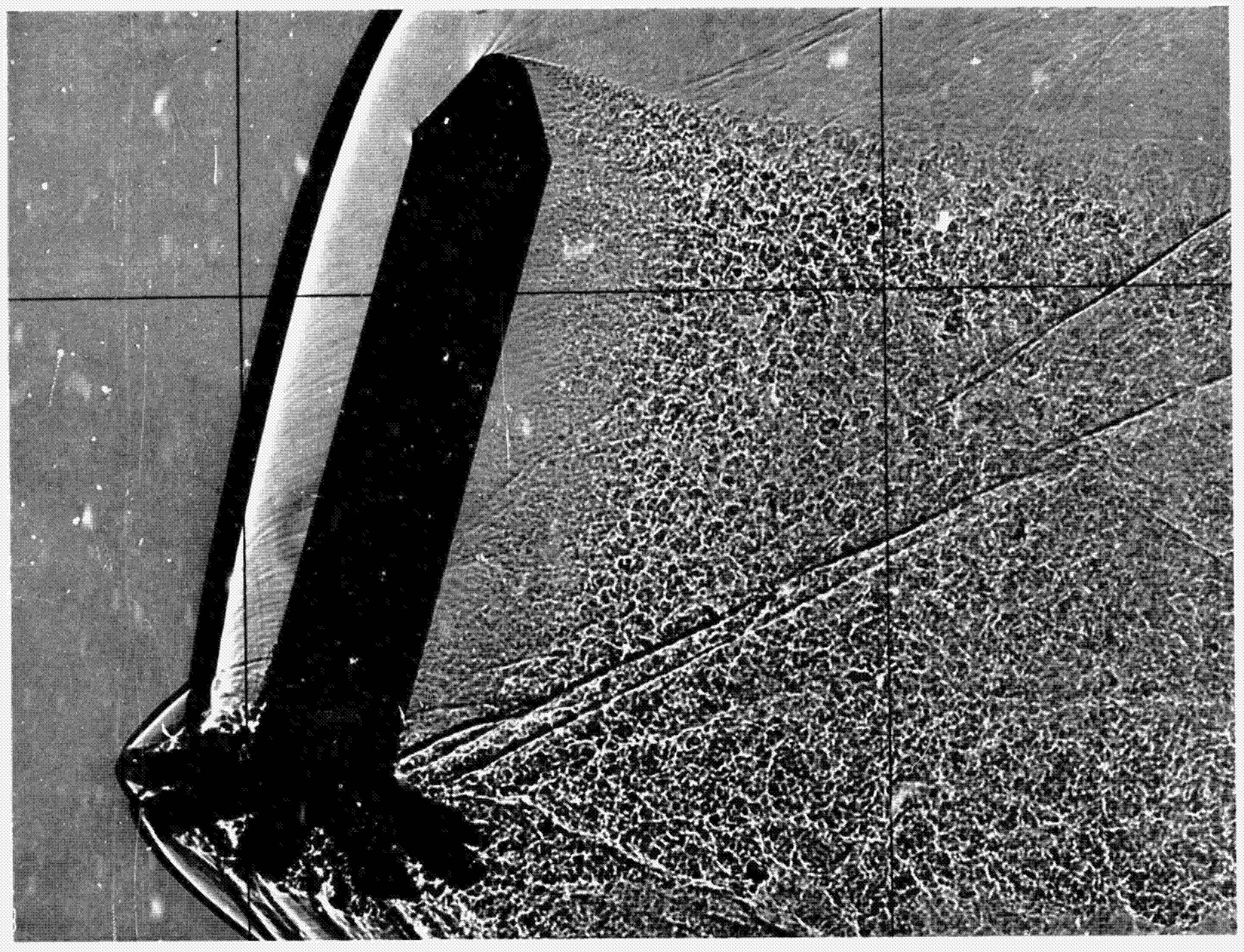

(b) 70°-panel model, M = 2.5, flight no. 1628, β = -105.4°, (α = -112.0°).

Figure 7.- Concluded.

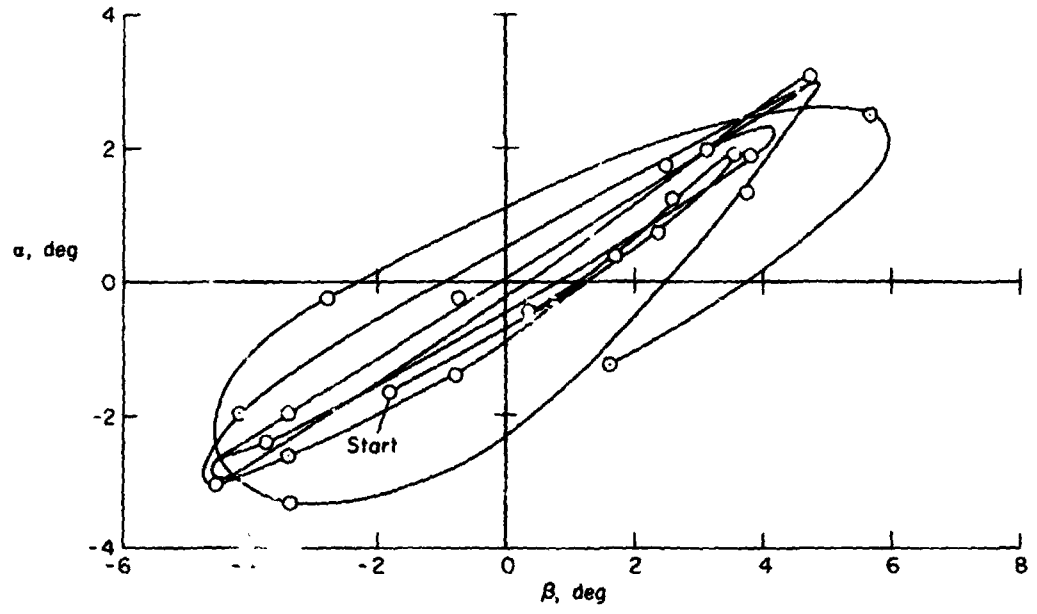

(a) 90°-panel model, M = 1.5, flight no. 1614.

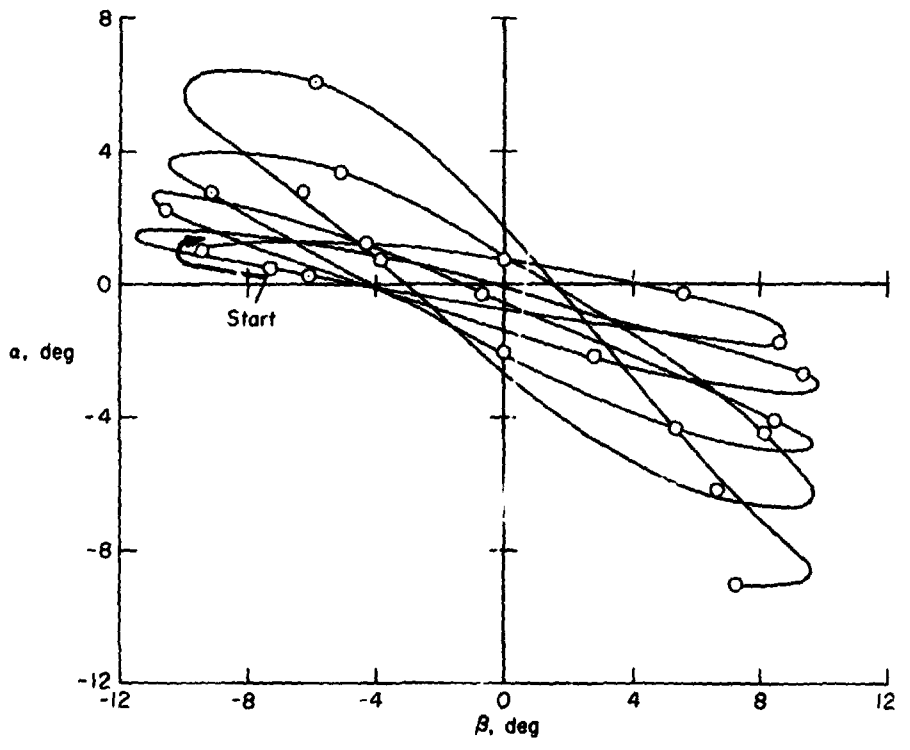

(b) 70°-panel model, M = 3.5, flight no. 1626.

Figure 8.- Typical angular motions of models.

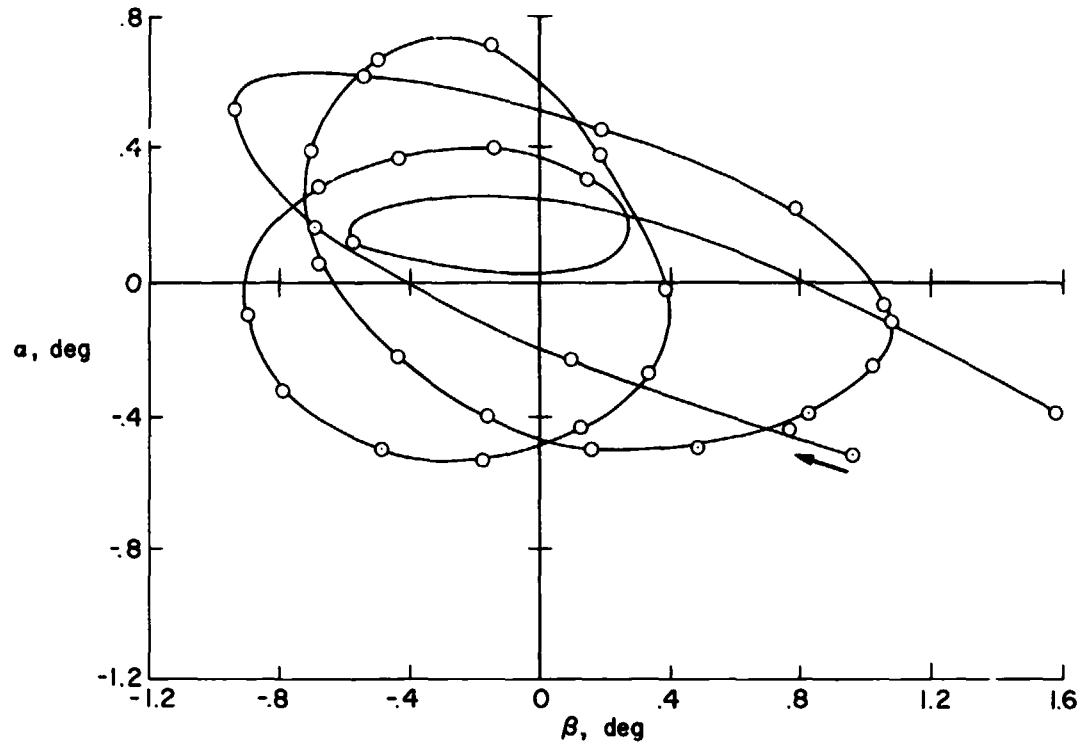

(c) 90°-panel model, M = 0.7, flight no. 1622.

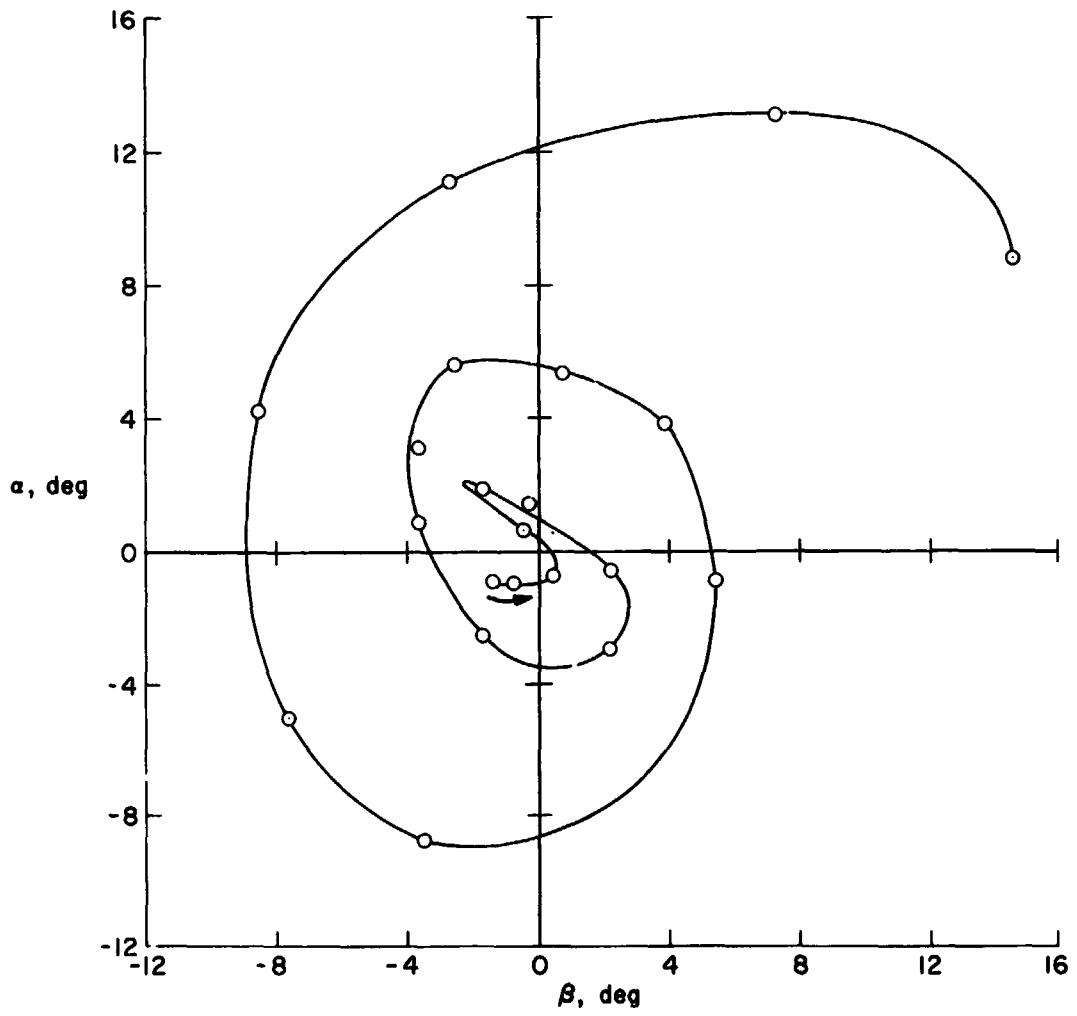

(d) 70°-panel model, M = 0.7, flight no. 1625.

Figure 8.- Continued.

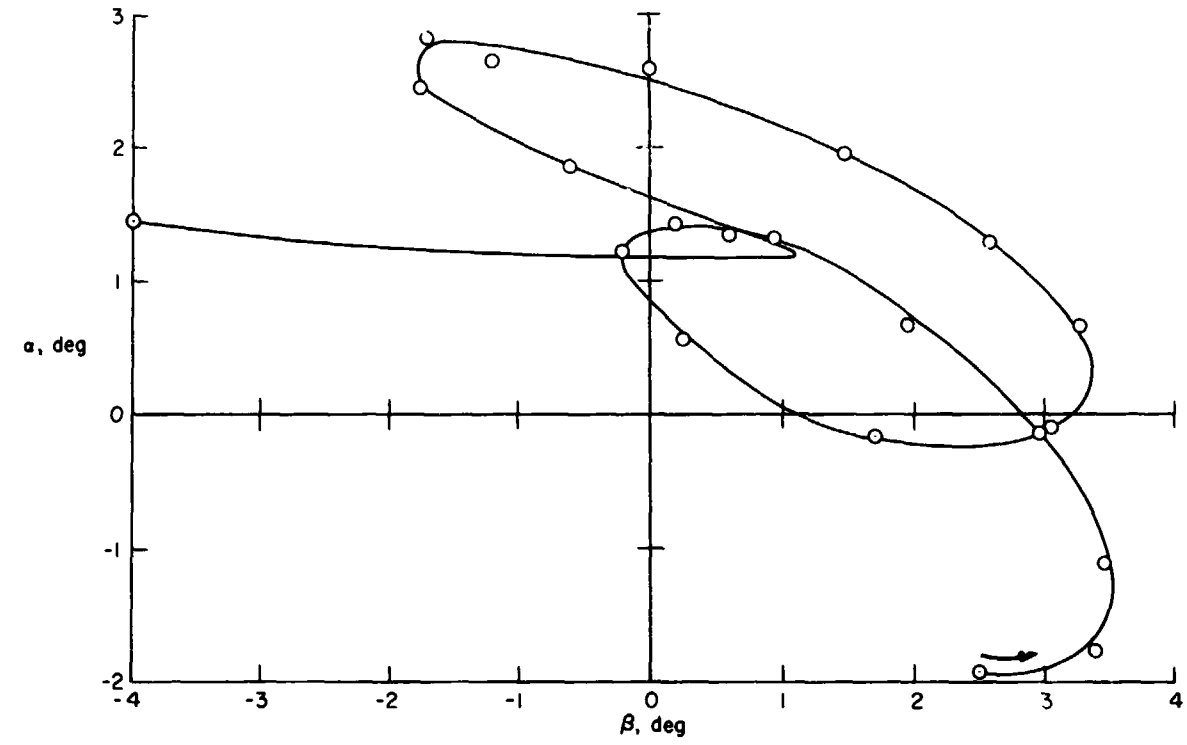

(e) 70°-panel model, M = 0.7, flight no. 1629.

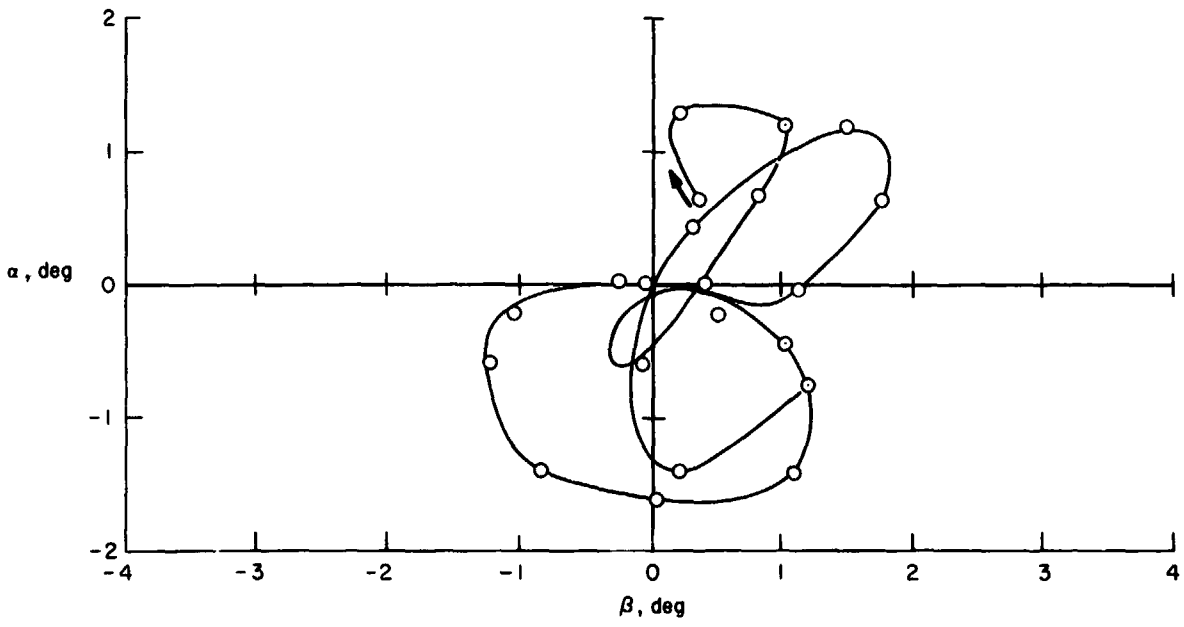

(f) 70°-panel model, M = 0.7, flight no. 1630.

Figure 8.- Concluded.

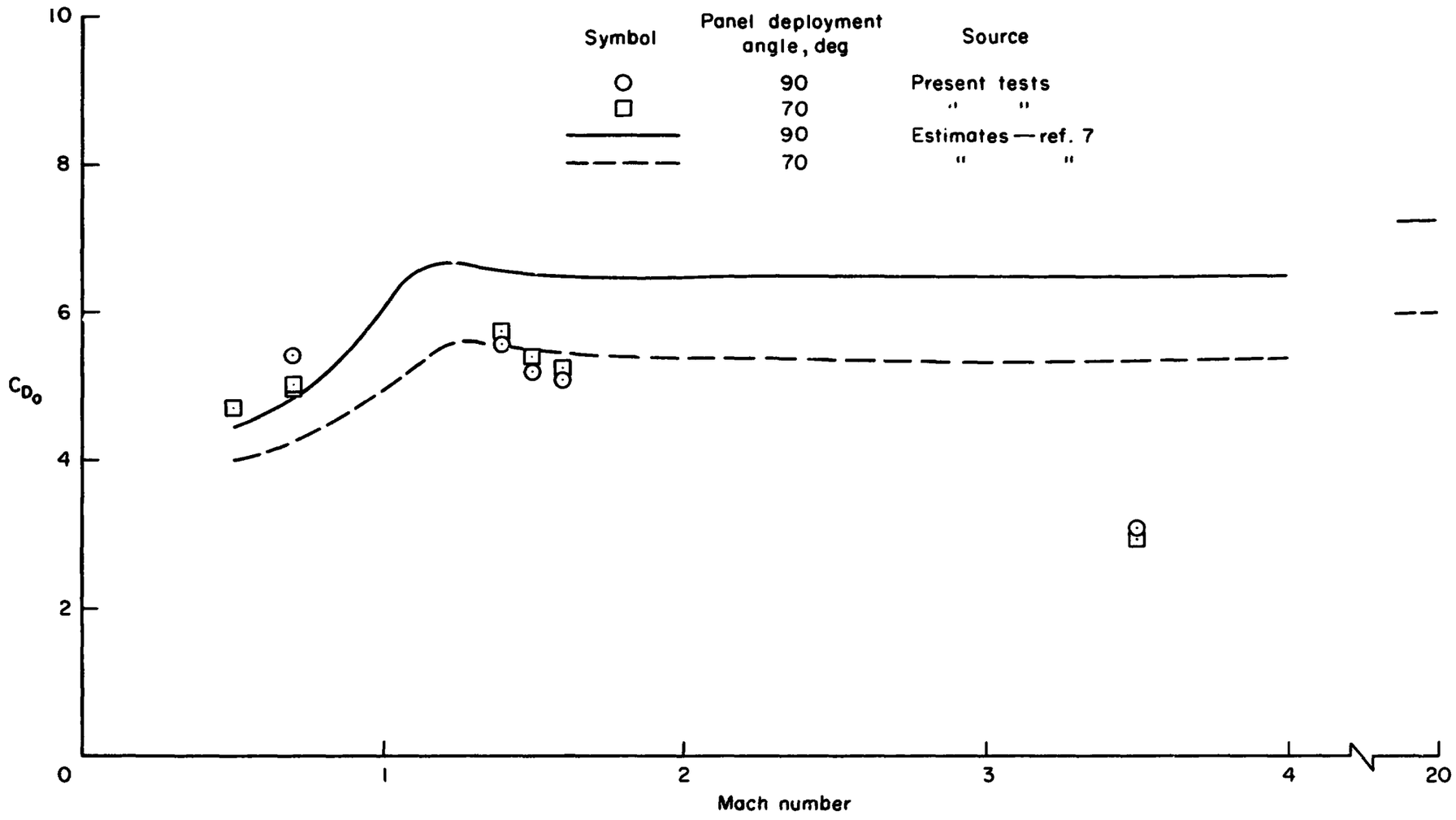

Figure 9.- Drag data.

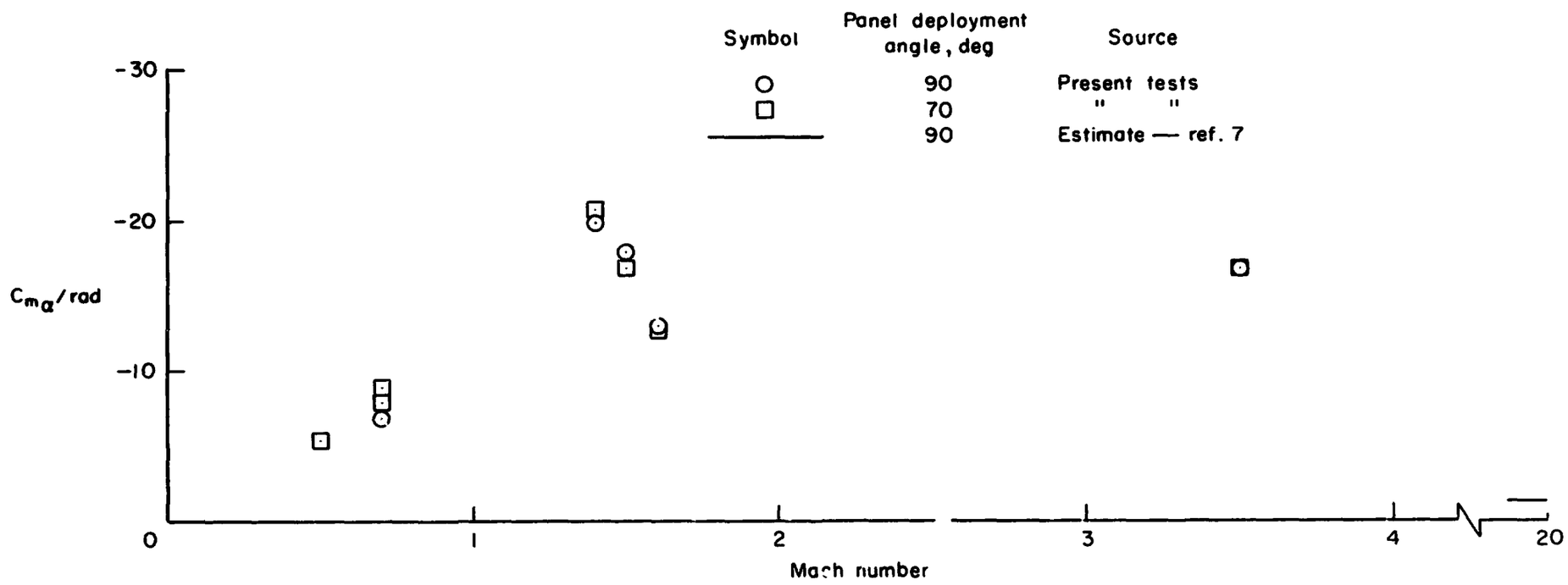

Figure 10.- Static stability data; $x_{cg}/d = 3.4$.

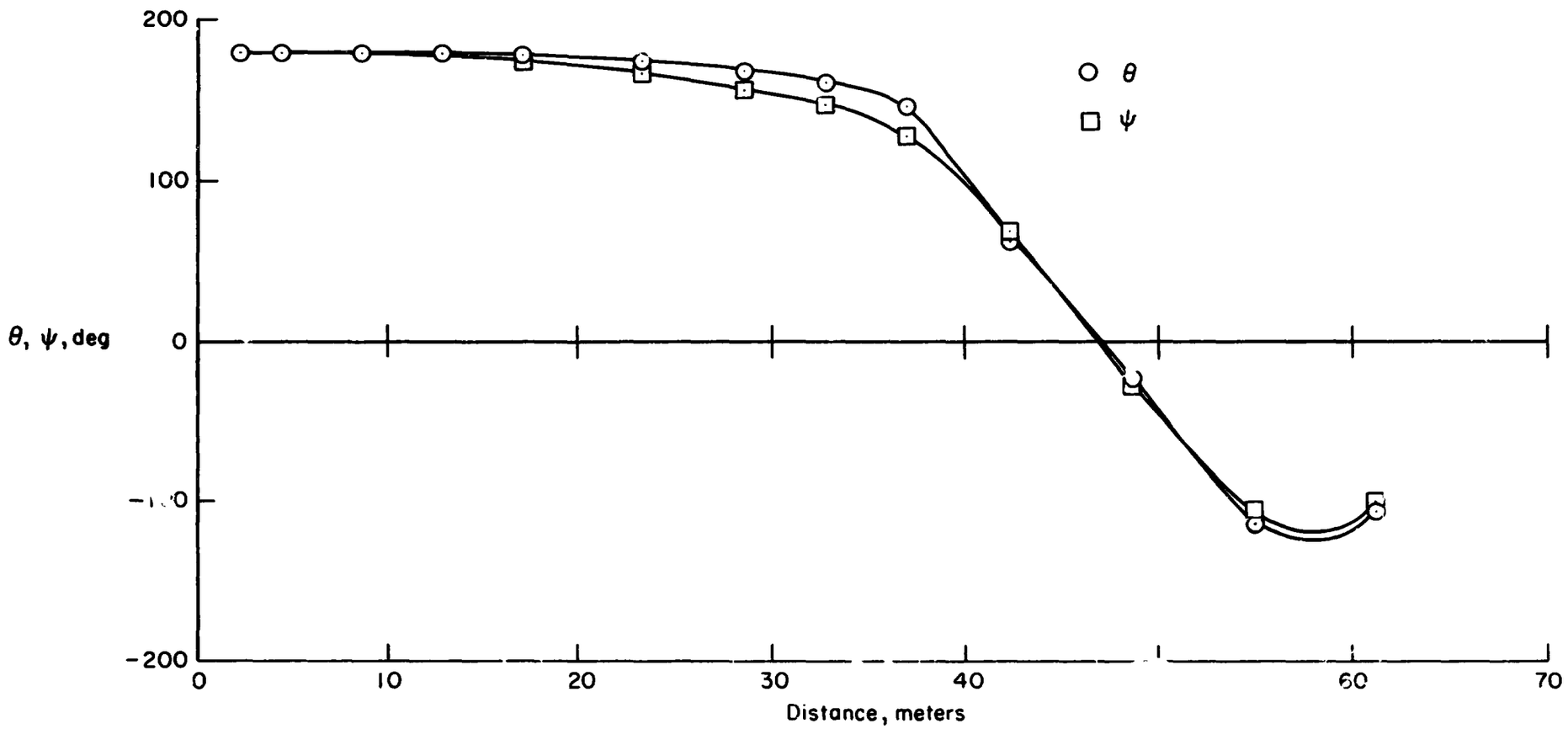

Figure 11.- Angular orientation - distance history of a 70°-panel model launched backwards (flight 1628); M = 2.5, Re = 0.22 x 10^6, x_{cg}/d = 3.4.